Supporting Information for

Three-dimensional Pyrene-fused *N*-Heteroacenes

Ben-Lin Hu, Cunbin An, Manfred Wagner, Georgia Ivanova, Anela Ivanova, Martin Baumgarten

Contents

Instrumentation

^{1}H NMR, ^{13}C NMR and 2D NMR spectra were recorded in deuterated solvents on a Bruker AVANCE 250, Bruker AVANCE III 300, AVANCE III 500, AVANCE III 700 and AVANCE III 850 spectrometer. Elemental analysis of solid samples was carried out on a Foss Heraeus Vario EL as a service of the Institute for Organic Chemistry, Johannes Gutenberg-University of Mainz. UV–Vis absorption spectra were measured on a Perkin-Elmer Lambda 900 spectrophotometer at room temperature. The fluorescence spectra were recorded on a SPEX-Fluorolog II (212) spectrometer. Cyclic Voltammetry (CV) was carried out on a computer-controlled GSTAT12 in a three-electrode cell in anhydrous tetrahydrofuran solution of *n*-Bu_4NPF_6 (0.1 M) with a scan rate of 100 mV/s at room temperature under argon. A Pt wire, a silver wire, and a glassy carbon electrode were used as the counter electrode, the reference electrode, and the working electrode, respectively. High resolution mass spectrometry was performed via atmospheric pressure chemical ionization (APCI) for HR-MS for A, and Maldi-Tof MS for the M1-M2 and P1-P3 were performed on a Bruker Reflex II-TOF spectrometer using a 337 nm nitrogen laser by matrix-assisted laser desorption/ionization (MALDI) with TCNQ (tetracyanoquinodimethane) as the matrix. The molecular weights were determined by PSS-WinGPC (PSS) (pump: alliance GPC 2000) GPC equipped with RI detector running in tetrahydrofuran at 30 ^{o}C using a PLgel MIXED-B column (particle size: 10 mm, dimension:0.8×30 cm) calibrated against polystyrene standards. Density functional theory (DFT) geometry optimization was performed initially with the B3LYP hybrid functionals[S1,S2] and basis set 6-31G *in vacuo* within the Gaussian 09 program[S3] package. Then, the structures were refined using the Gaussian 16 program[S4] at the B3LYP/6-31G(d) level and vibrational frequencies calculations verified the minima. The electronic absorption spectra were computed for the B3LYP/6-31G(d) optimized geometries with TD-DFT using the TPSSh[S5] functional and the same basis set. 60 excited states were included in the calculation. The solvent tetrahydrofuran was included implicitly by PCM.[S6]

Reagents and synthesis

2,7-Ditert-butyl-pyrene-4,5,9,10-tetraone **S1**[S7] and 5,6-diamine-4,7-bis((triisopropylsilyl)ethynyl)benzo[*c*][1,2,5]thiadiazole **S2**[S8] were prepared according to the reported procedures. All starting chemicals, unless otherwise specified, were purchased from Alfa Aesar or Sigma-Aldrich and used as received. Solvents were purified by normal

procedure before use. The other materials were common commercial level and used as received.

Scheme 1. The synthesis of **A**.

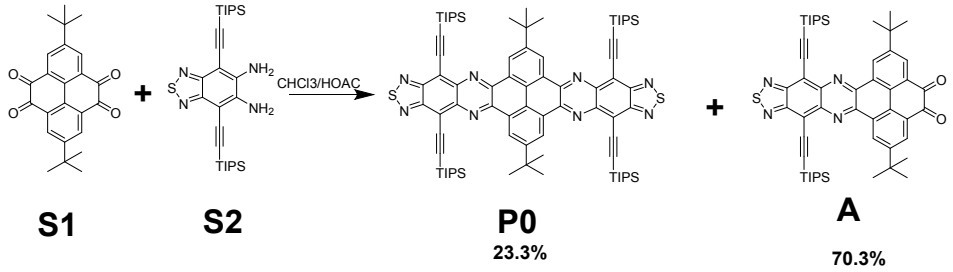

P0 and A

2,7-Di-t-butylpyrene-4,5,9,10-tetraone **S1** (411 mg, 1.1 mmol) and 5,6-diamine-4,7-bis((triisopropylsilyl)ethynyl)benzo[*c*][1,2,5]thiadiazole **S2** (304 mg, 0.57 mmol) were dissolved in 132 mL of chloroform and 33 mL of glacial acetic acid. The mixture was refluxed overnight under argon. The reaction mixture was cooled to room temperature and washed with H_2O and 10% NaOH (aq). The organic layer was collected and dried over Na_2SO_4. The MgSO4 was filtered out and rinsed with methylene chloride. The solvent was removed under vacuum to yield the crude product which was purified by silica gel column chromatography (CH_2Cl_2/hexane, 1/2 v/v). The pure product **P0** and A were obtained. P0, red solid, 92 mg, yield 23.3% (based on **S2**), Rf = 0.756 (DCM/hex = 1/1 v/v). The ^{1}H NMR agrees with the data reported.[S9]

A: red solid, 347 mg, yield 70.3% (based on **S2**), Rf = 0.20 (CH_2Cl_2/hexane, 1/1 v/v). ^{1}H NMR (300 MHz, CD_2Cl_2, δ ppm): 9.74 (d, J = 2.2 Hz, 2H), 9.61 (d, J = 2.2 Hz, 2H), 1.57 (s, 18H), 1.40-1.30 (m, 42H). ^{13}C (75 MHz, CD_2Cl_2, δ ppm): 180.43, 156.16, 153.77, 144.60, 141.72, 131.49, 131.33, 130.99, 130.74, 130.21, 115.16, 111.56, 102.35, 36.02, 31.53, 19.33, 12.24. HRMS (APCI): *m*/*z* calcd for $C_{52}H_{65}N_4O_2SSi_2$ $[M+H]^+$, 856.4361, found 865.4361. elemental analysis calcd (%) for $C_{52}H_{64}N_4O_2SSi_2$:C72.18, H7.46, N6.47, S3.70; found: C72.20, H7.46, N6.49, S3.72.

P1

The intermediate **A** (60 mg, 0.07 mmol), 2,3,6,7,14,15-hexaammoniumtriptycene hexachloride **B** (12.6 mg, 0.022 mmol) and KOAc (18 mg, 0.18 mmol) were added into a mixture of chlorobenzene (4 mL) and acetic acid (2 mL), and the mixture was heated to reflux under argon for two days. After the mixture cooling to room temperature, all the solvents

were removed under vacuum. The residues were elute by silica gel column chromatography to obtain **P1** (eluted with DCM/hexane=1/2 v/v). P1, red solid, 63 mg, yield 100% based on B, Rf = 0.34 (DCM/hexane=1/2 v/v). ^{1}H NMR (700 MHz, CD_2Cl_2, δ ppm): 9.86 (d, J = 2.1 Hz, 6H), 9.85 (d, J = 2.1 Hz, 2H), 8.75 (s, 6H), 6.57 (s, 2H), 1.75 (s, 54H), 1.39-1.31 (m, 126H). ^{13}C (175 MHz, CD_2Cl_2, δ ppm): 155.98, 152.04, 146.29, 144.65, 143.13, 142.46, 142.06, 130.27, 129.70, 127.05, 126.82, 126.41, 124.94, 114.72, 110.70, 102.55, 54.07, 36.31, 31.53, 19.33, 12.24. MALDI-TOF MS: **Figure S20**. elemental analysis calcd (%) for $C_{176}H_{200}N_{18}S_3Si_6$: C74.64, H7.12, N8.90, S3.40; found: C74.62, H7.13, N8.89, S3.43.

M1

Compound **P1** (60 mg, 0.0211 mmol) was dissolved in dry THF (5 mL) under argon and stirred at 0 ℃. Then $LiAlH_4$ (1.26 mL, 1 M in THF, 1.26 mmol, 60 eq) was slowly added. After that, the reaction mixture was allowed to warm to room temperature and stirred overnight. The reaction was quenched with saturated, aqueous NH_4Cl solution. The mixture was extracted with ether (30 mL×2). The combined organic layers were dried over $MgSO_4$ and concentrated under reduced pressure to afford compound **M1** as yellow solid with strongly bright yellow fluorescence (~50 mg,). ^{1}H NMR (250 MHz, CD_2Cl_2, δ ppm): 9.82 (s, 6H), 9.80 (s, 6H), 8.73 (s, 6H), 6.54 (s, 2H), 5.01 (s, 12H), 1.75 (s, 54H), 1.38-1.31 (m, 126H). The ^{1}H NMR shows that a little THF was left inside and the product can be used for the next reaction directly without further purification. This compound is not stable, even in the fridge, so it is better to use as soon as possible. MALDI-TOF MS: **Figure S21**.

P2

M1 (50 mg) and the intermediate **A** (56.83 mg) were dissolved in chlorobenzene (4 mL) and acetic acid (2 mL), and the mixture was heated to reflux under argon for two days. After the mixture cooling to room temperature, all the solvents were removed under vacuum. The residues were elute by silica gel column chromatography (DCM/hex = 1:2, Rf = 0.16) to obtain the product as a dark red solid (88 mg, yield 80.0 % based on P1 for two steps)

^{1}H NMR (500 MHz, $C_2D_2Cl_4$, 393K, δ ppm): 9.99 (s, 24H), 8.83 (s, 6H), 6.57 (s, 2H), 1.91 (s, 54H), 1.86 (s, 54H), 1.53-1.42 (m, 252H).^{1}H NMR (300 MHz, THF-d_8, δ ppm): 10.00 (s, 24H), 8.87 (s, 6H), 6.75 (s, 2H), 1.84 (s, 54H), 1.81 (s, 54H), 1.49-1.35 (m, 252H).

^{13}C (125 MHz, $C_2D_2Cl_4$, 393K, δ ppm): 155.44, 151.93, 151.42, 145.27, 145.03, 144.45, 143.76, 142.67, 142.34, 142.24, 141.89, 141.45, 129.81, 129.59, 129.51, 129.35, 127.36, 127.29, 127.12, 126.38, 126.23, 125.59, 124.22, 121.89, 114.48, 110.59, 110.52, 103.17, 102.29, 53.87, 35.62, 36.49, 31.63, 31.55, 18.91, 18.80, 12.29, 11.76. MALDI-TOF MS: **Figure S22**. elemental analysis calcd (%) for $C_{332}H_{392}N_{30}S_3Si_{12}$: C76.16, H7.55, N8.03, S1.84; found: C76.15, H7.55, N8.04, S1.83.

M2

The procedure is as that for M1.60 P1 (42 mg) in THF (5 mL), $LiAlH_4$ (2.4 mL, 1 M in THF, 2.4 mmol, 300 eq) Yellow solid strongly bright yellow fluorescence. ^{1}H NMR (250 MHz, CD_2Cl_2, δ ppm): 9.94 (s, 12H), 9.90 (d, J = 1.875 Hz, 6H), 9.87 (d, J = 1.875 Hz, 6H), 8.79 (s, 6H), 6.60 (s, 2H), 5.00 (s, 12H), 1.82 (s, 54H), 1.76 (s, 54H), 1.36-1.23 (m, 126H). MALDI-TOF MS: **Figure S23**.

P3

The procedure is as that for P2. **M2** (~40 mg) and the intermediate **A** (24.29 mg) were dissolved in chlorobenzene (4 mL) and acetic acid (2 mL). red solid, 40 mg, yield 71%.

^{1}H NMR (500 MHz, $C_2D_2Cl_4$, 413K, δ ppm): 10.03 (s, 12H), 10 (s, 24H), 8.82 (s, 6H), 6.55(s, 2H), 1.92 (s, 108H), 1.88 (s, 54H), 1.59-1.42 (m, 378H).

^{13}C (125 MHz, $C_2D_2Cl_4$, 413K, δ ppm): 155.47, 153.41, 152.03, 151.89, 151.47, 145.30, 145.02, 144.72, 144.58, 144.53, 143.79, 142.71, 142.37, 142.30, 141.94, 141.48, 130.69, 130.23, 129.83, 129.76, 129.70, 129.64, 129.55, 129.42, 127.39, 127.34, 127.28, 127.18, 126.41, 126.21, 125.61, 124.20, 121.98, 121.91, 114.52, 110.77, 110.69, 110.56, 103.29, 103.24, 102.36, 102.04, 53.98, 35.62, 35.52, 35.51, 18.90, 18.75, 18.68, 12.33, 11.80, 11.73. MALDI-TOF MS: **Figure S24**. elemental analysis calcd (%) for $C_{488}H_{584}N_{42}S_3Si_{18}$:C76.72, H7.71, N7.70, S1.26; found: C76.73, H7.71, N7.69, S1.26.

P4

Compound **P3** (32 mg, 4.19 μmol) was dissolved in dry THF (20 mL) under argon and stirred at 0 ℃. Then $LiAlH_4$ (1.89 mL, 1 M in THF, 1.89 mmol, 450 eq) was slowly added. After that, the reaction mixture was allowed to warm to room temperature and stirred overnight. The reaction was quenched with saturated, aqueous NH_4Cl solution. The mixture was extracted with ether (30 mL × 2). The combined organic layers were dried over $MgSO_4$ and

concentrated under reduced pressure to afford a red solid, which is used in the next step directly. The obtained red solid and the intermediate **A** (12.85 mg, 14.7 μmol) were dissolved in chlorobenzene (6 mL) and acetic acid (2 mL), and the mixture was heated to reflux under argon for two days. After the mixture cooling to room temperature, the solid was filtered and washed with DCM and THF, and the product was obtained as a dark red solid (11 mg, yield 26.2 % based on P3 for two steps). ^{1}H NMR (500 MHz, $C_2D_2Cl_4$, 413K, δ ppm): 10.13-9.81 (m, 48H), 8.81 (s, 6H), 6.55 (s, 2H), 1.98-1.81 (m, 216H), 1.58-1.34 (m, 504H). elemental analysis calcd (%) for $C_{644}H_{776}N_{54}S_3Si_{24}$: C77.01, H7.79, N7.53, S0.96; found: C77.00, H7.78, N7.54, S0.96.

NMR spectra of all new compounds

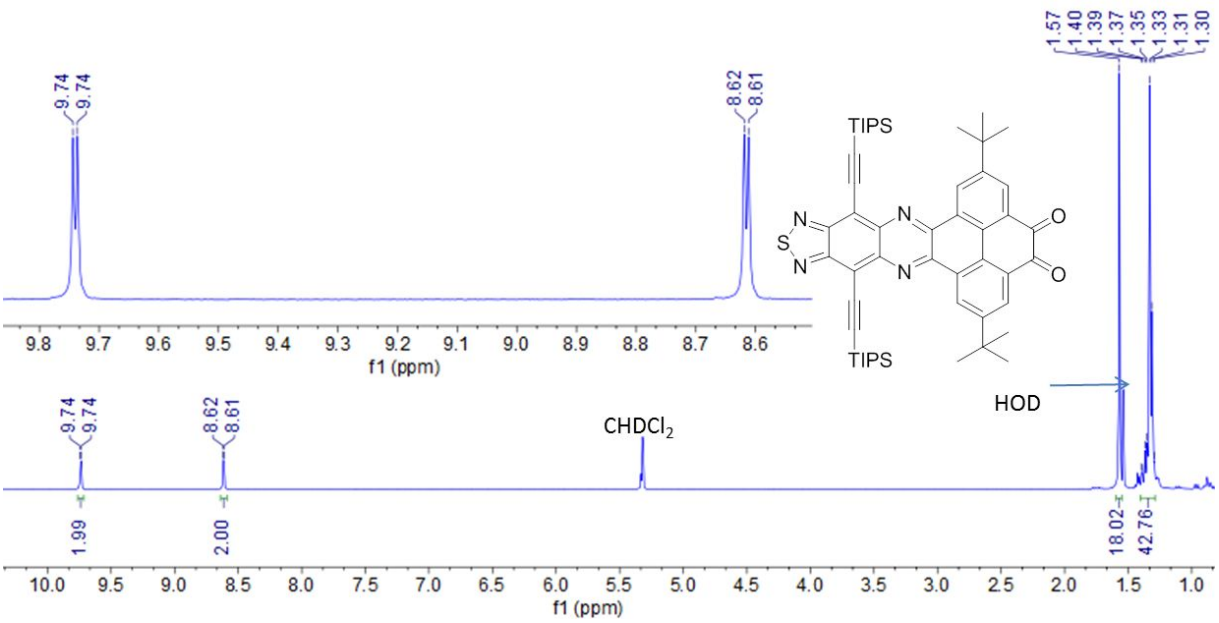

Figure S1. The ^{1}H NMR spectrum of compound **A** in 1,1,2,2-tetrachloroethane-d_2 on 250 MHz.

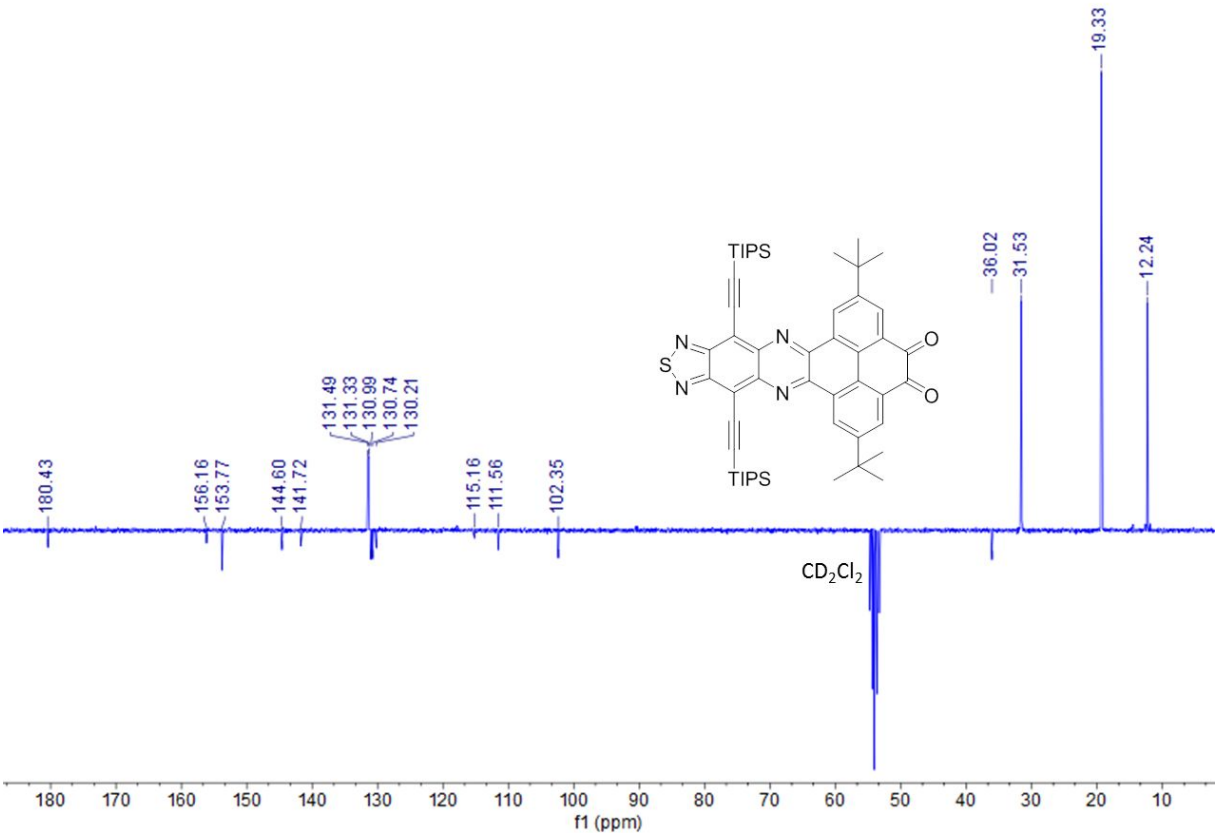

Figure S2. The APT ^{13}C NMR spectrum of compound **A** in CD_2Cl_2 on 75 MHz.

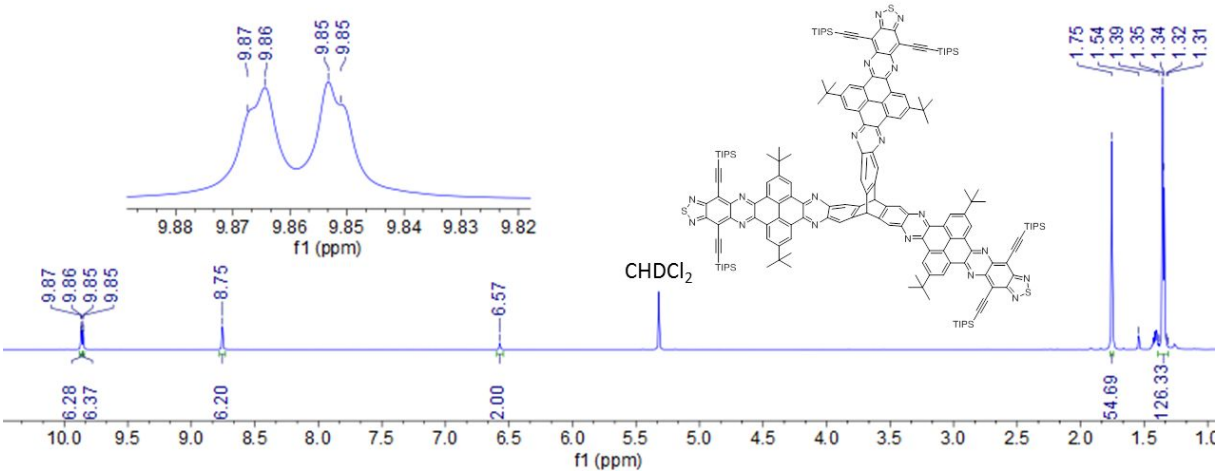

Figure S3. The ^{1}H NMR spectrum of compound **P1** in CD_2Cl_2 on 700 MHz.

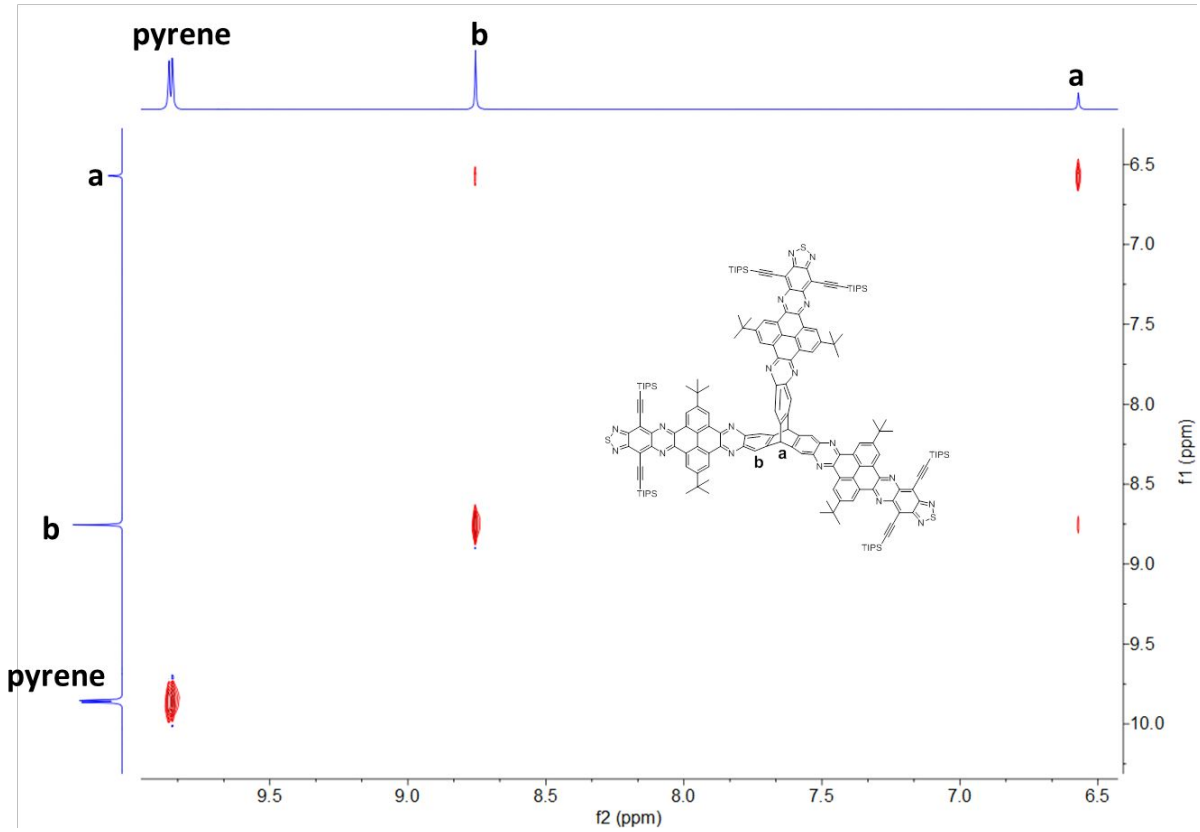

Figure S4. The aromatic region of the ^{1}H–^{1}H NOESY spectrum of compound **P1** in CD_2Cl_2 on 700 MHz.

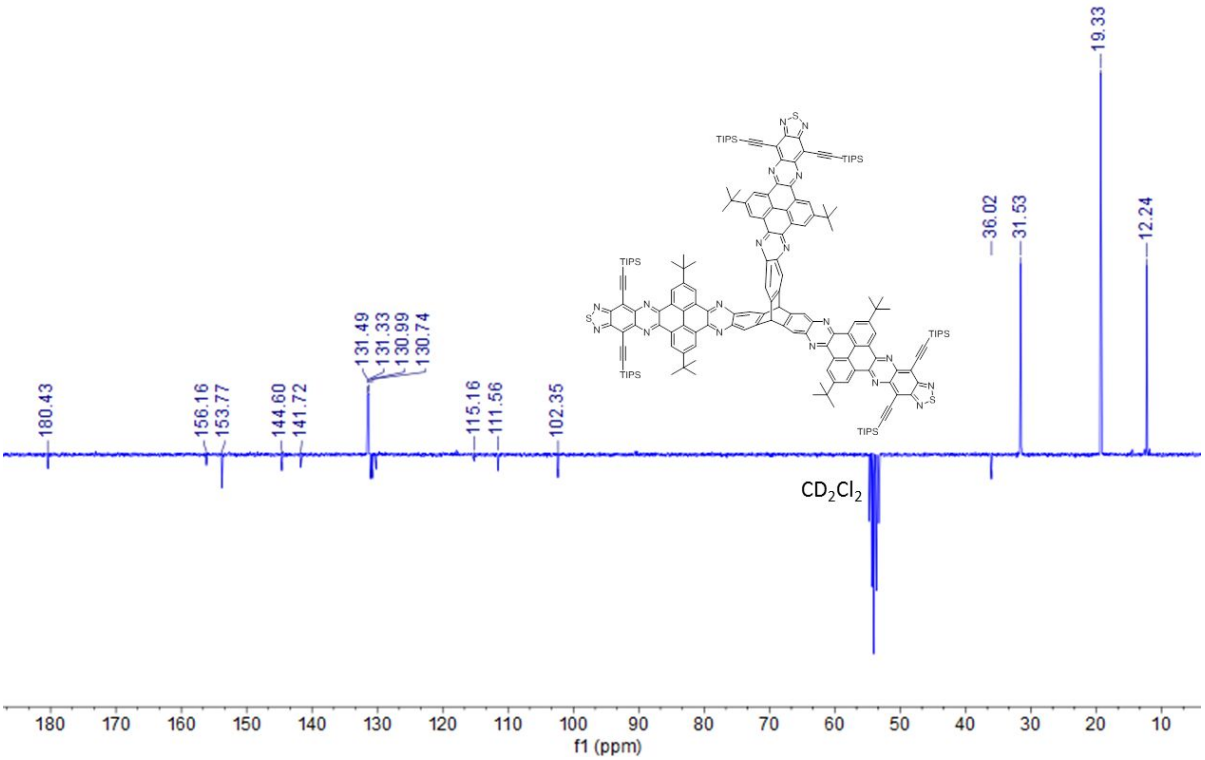

Figure S5. The APT ^{13}C NMR spectrum of compound **P1** in CD_2Cl_2 on 175 MHz.

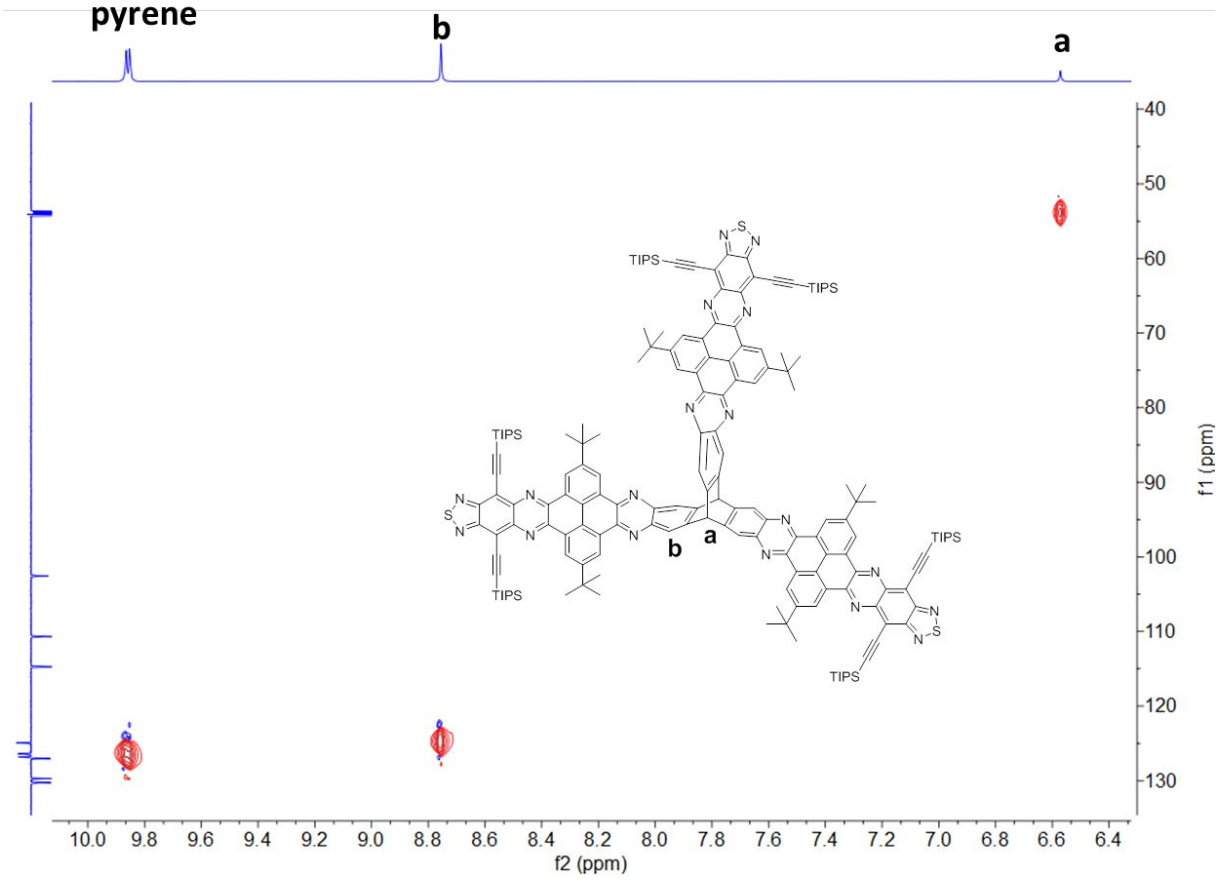

Figure S6. The aromatic region of the ^{1}H-^{13}C HSQC spectrum of compound **P1** in CD_2Cl_2.

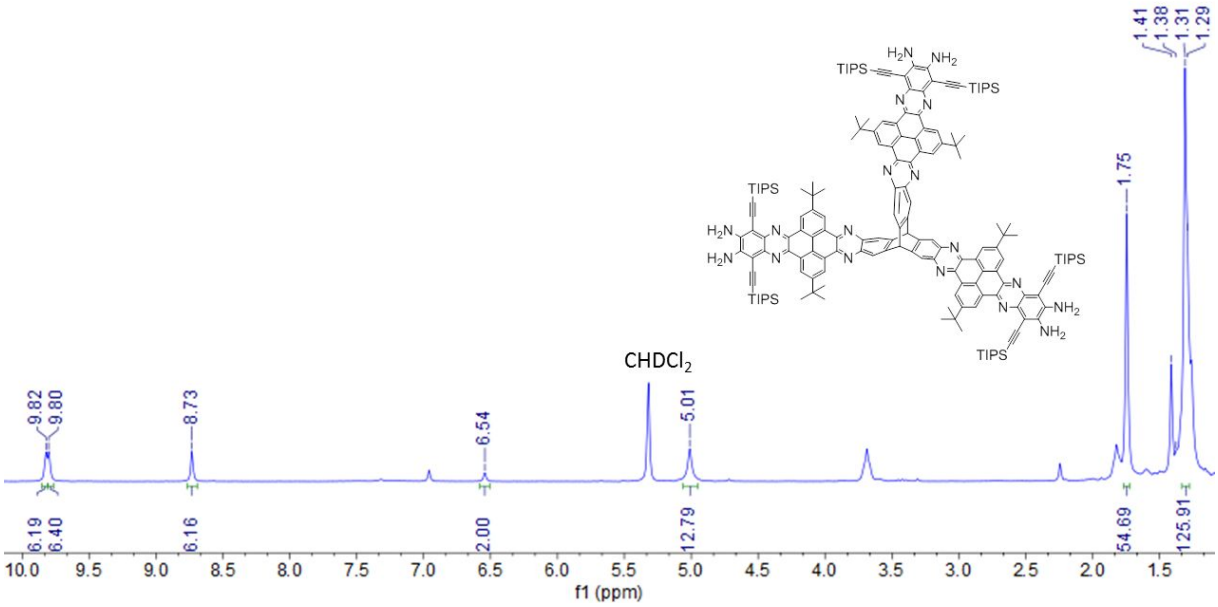

Figure S7. The ^{1}H NMR spectrum of compound **M1** in CD_2Cl_2 on 250 MHz.

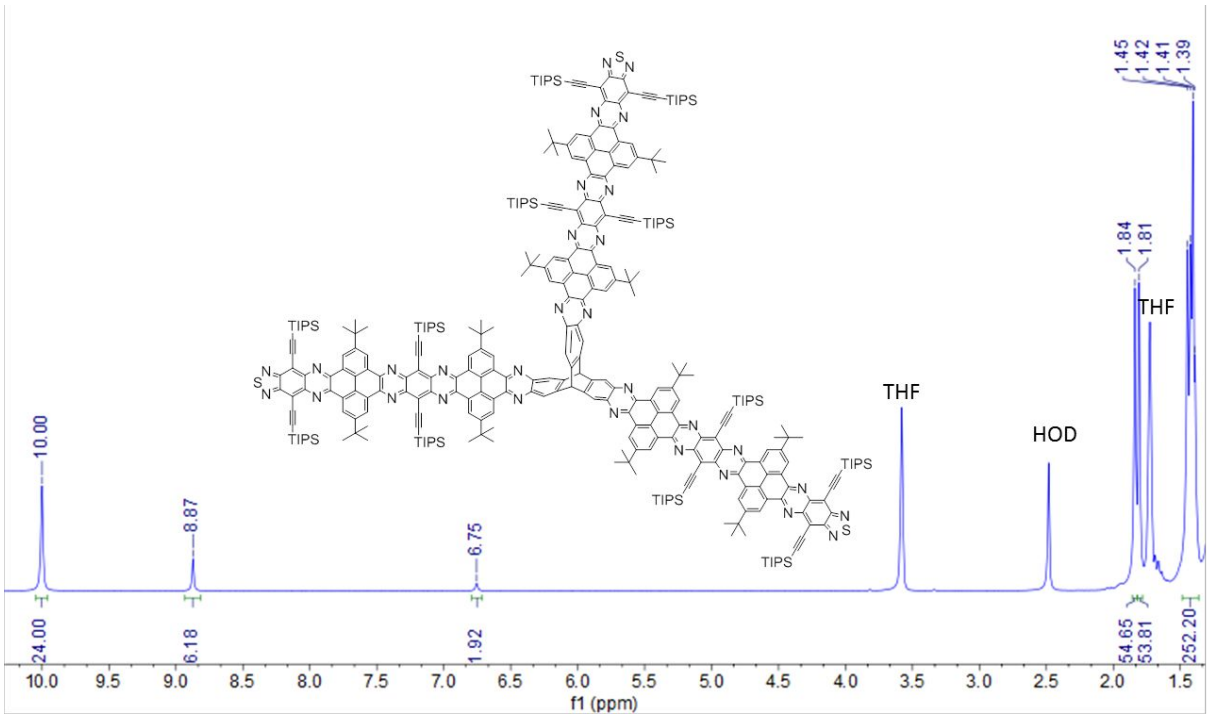

Figure S8. The ^{1}H NMR spectrum of compound **P2** in THF-d_8 on 300 MHz.

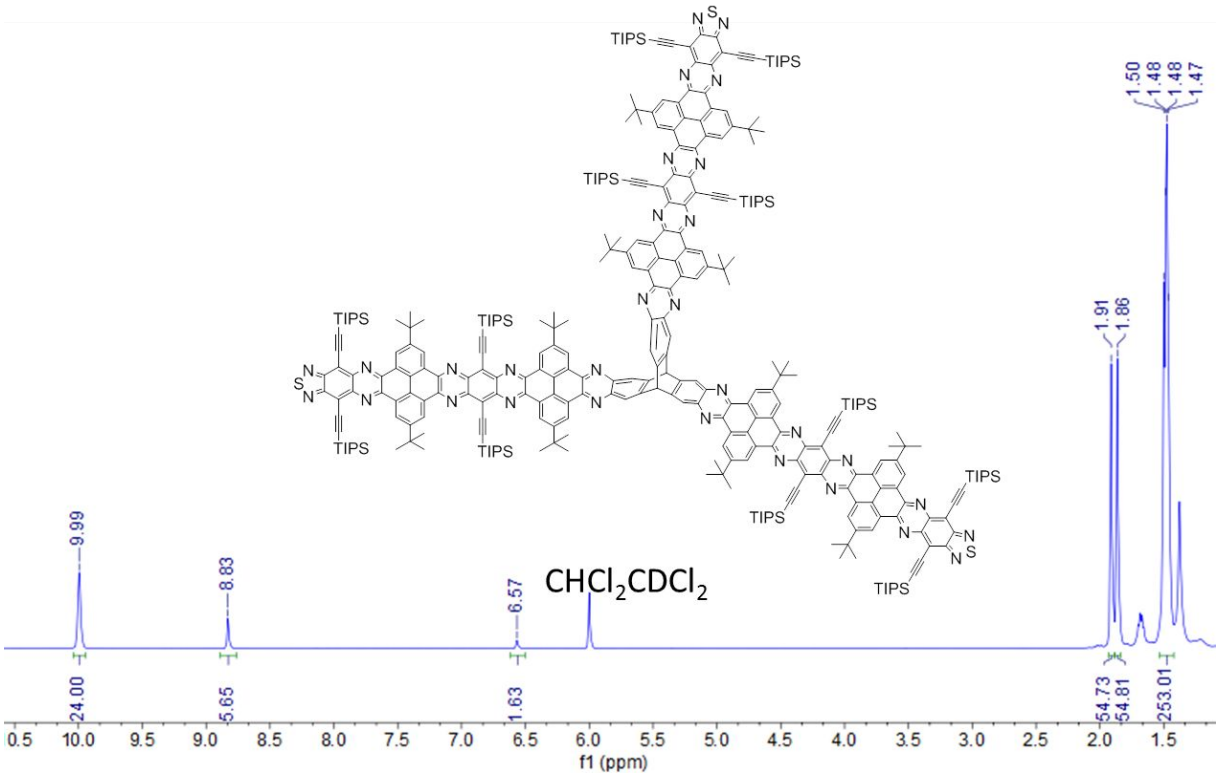

Figure S9. The ^{1}H NMR spectrum of compound **P2** in TCE-d_2 on 500 MHz at 393 K.

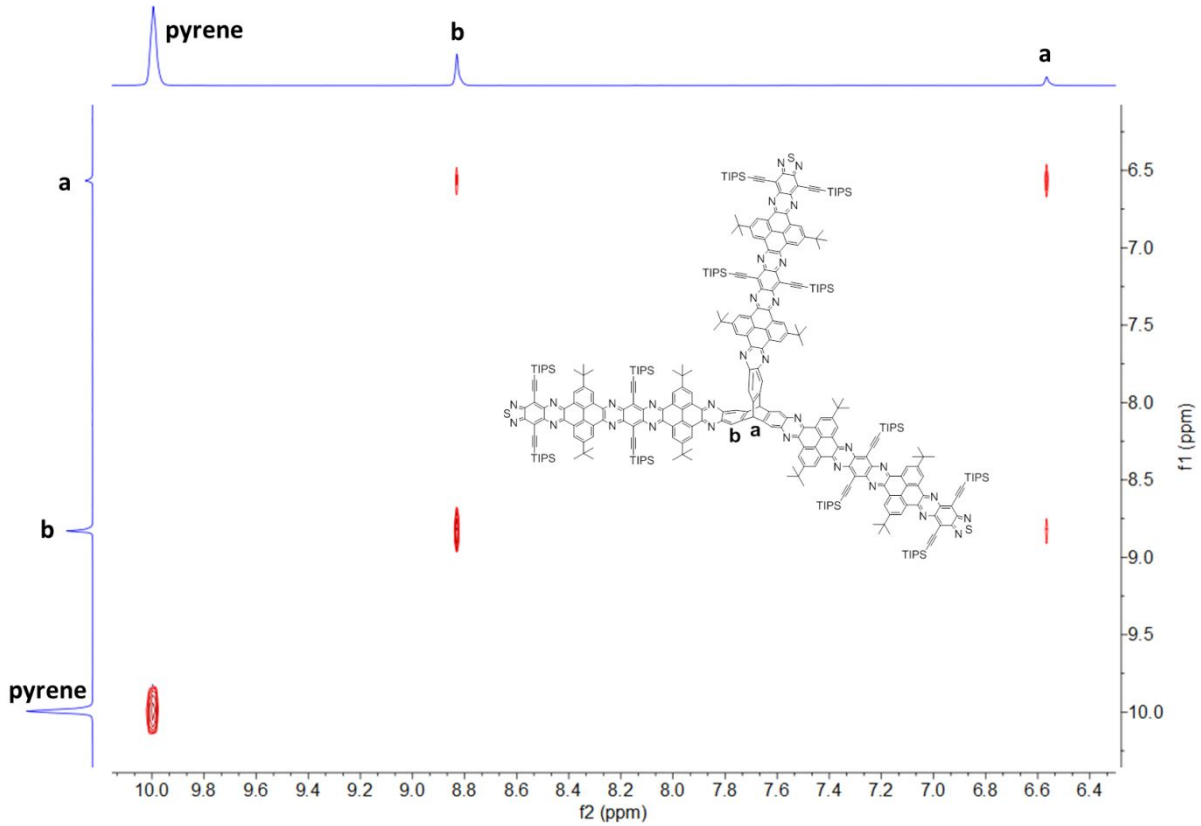

Figure S10. The aromatic region of the ^{1}H–^{1}H NOESY spectrum of compound **P2** in TCE-d_2 on 500 MHz at 393 K.

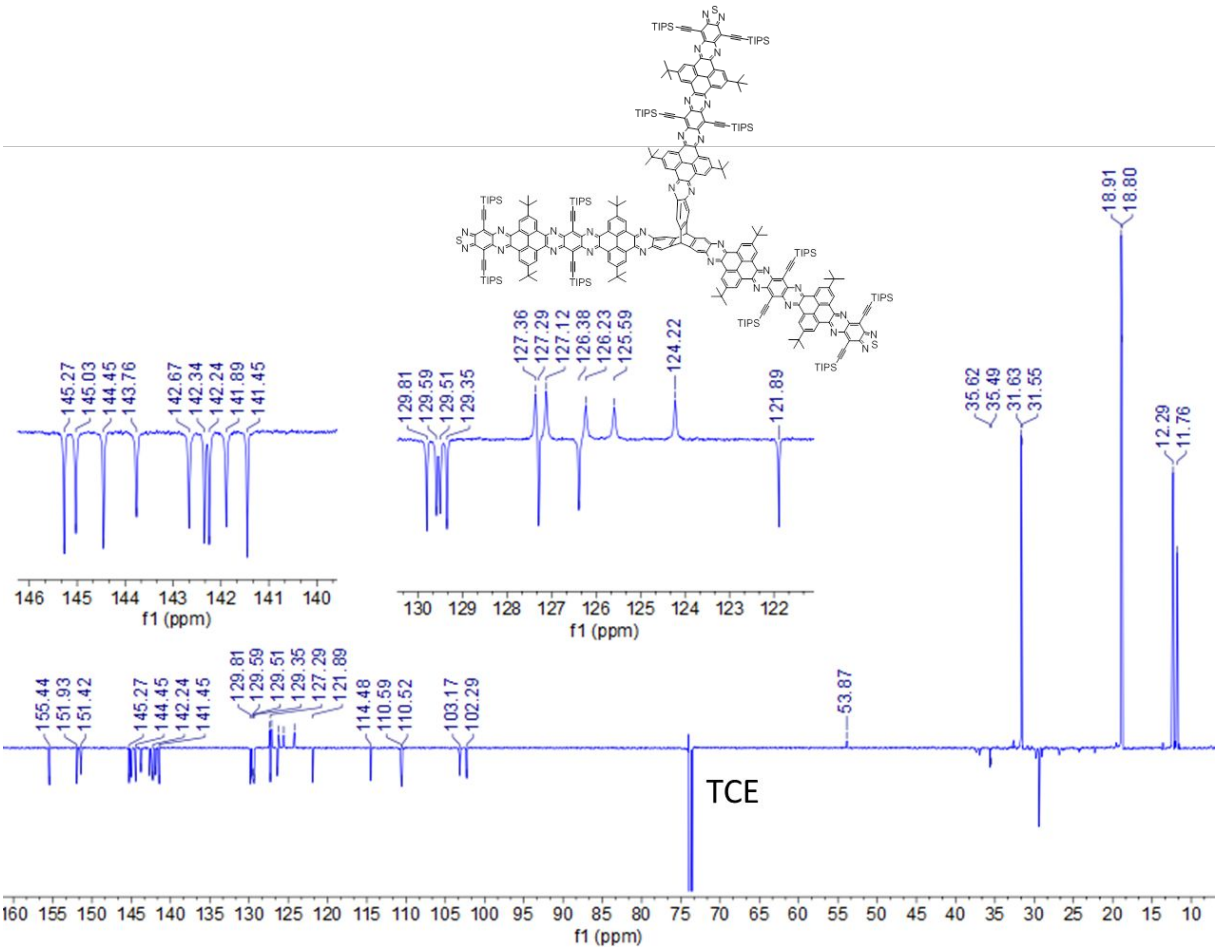

Figure S11. The APT ^{13}C NMR spectrum of compound **P2** in TCE-d_2 on 125 MHz at 393 K.

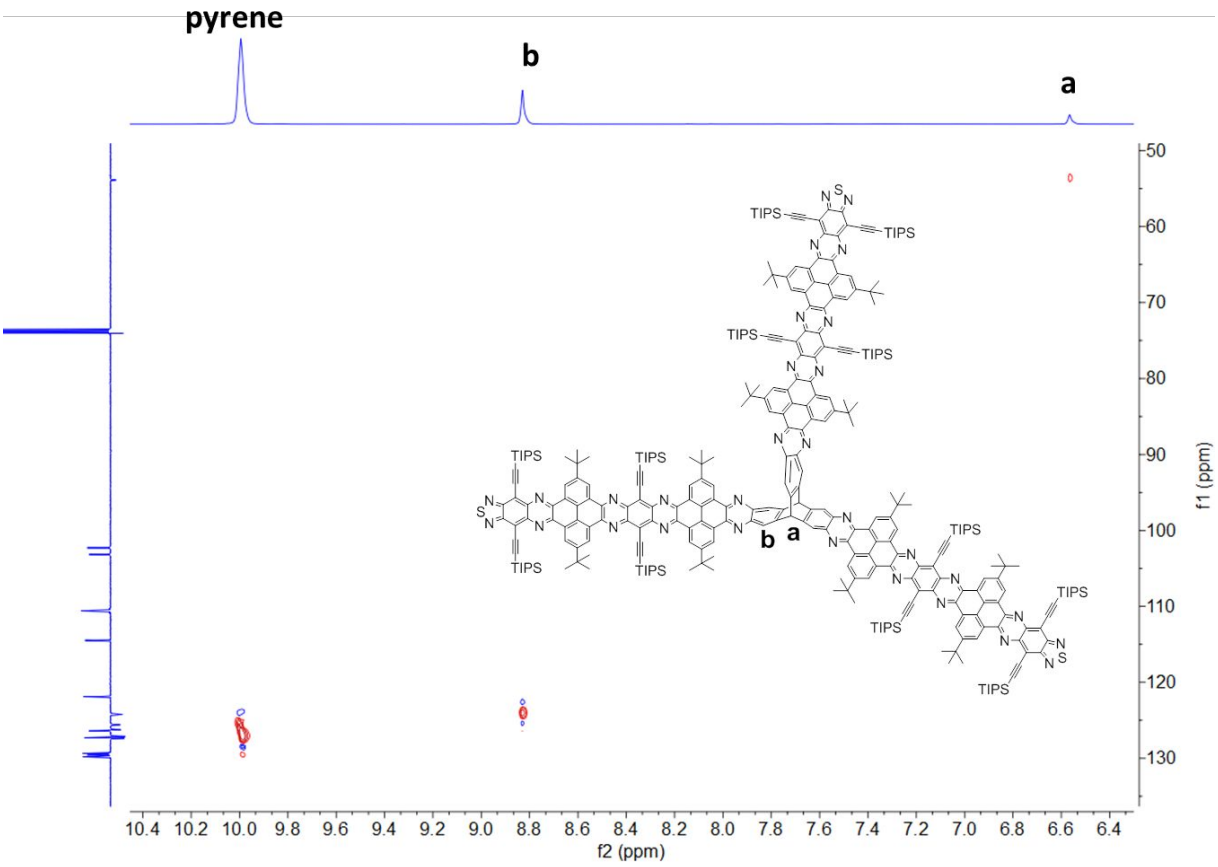

Figure S12. The aromatic region of the ^{1}H-^{13}C HSQC spectrum of compound **P2** TCE-d_2 at 393 K.

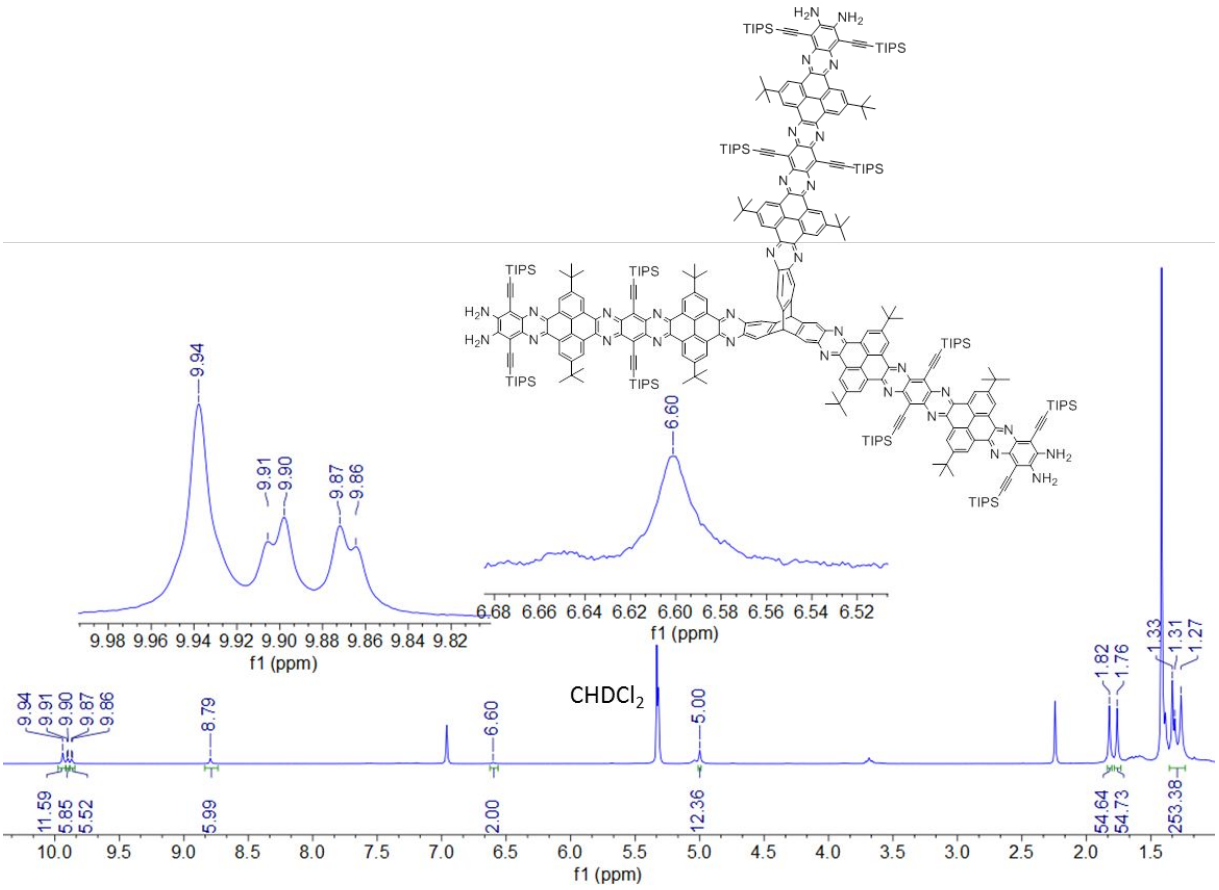

Figure S13. The ^{1}H NMR spectrum of compound **M2** in CD_2Cl_2 on 250 MHz.

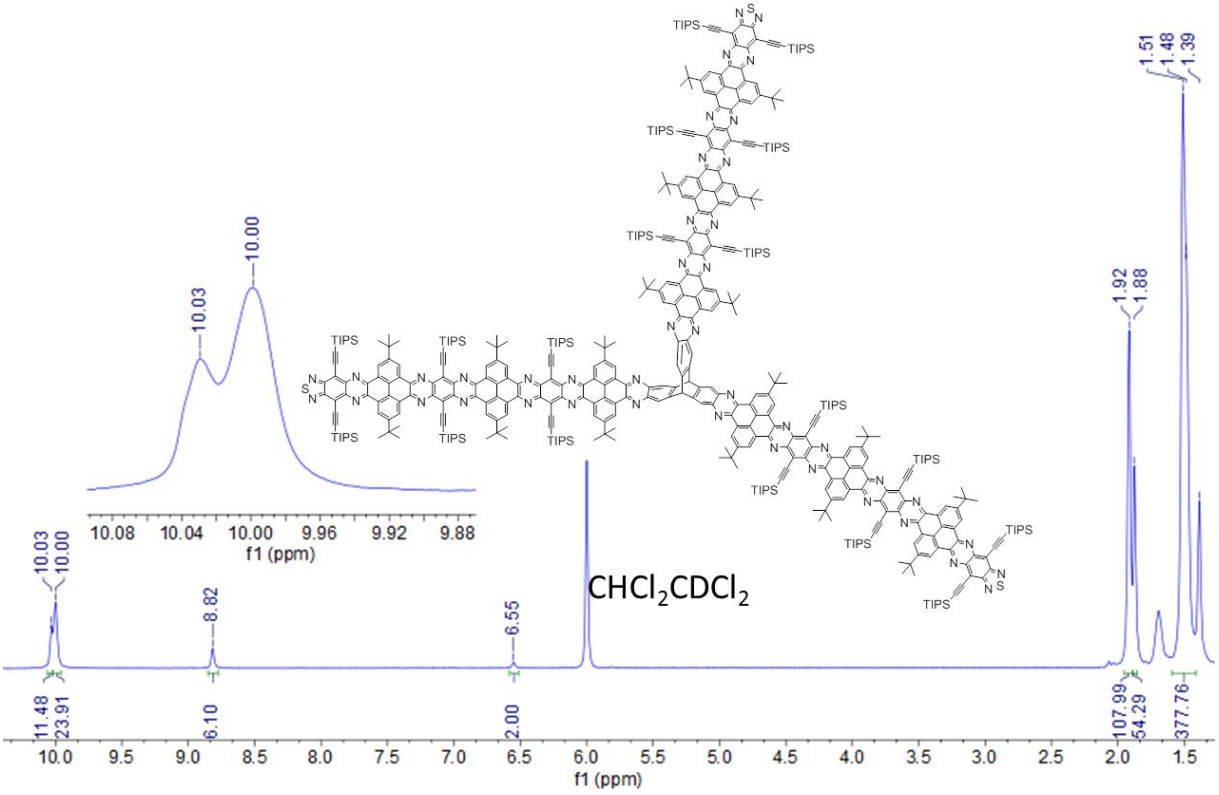

Figure S14. The ^{1}H NMR spectrum of compound **P3** in TCE-d_2 on 500 MHz at 413 K.

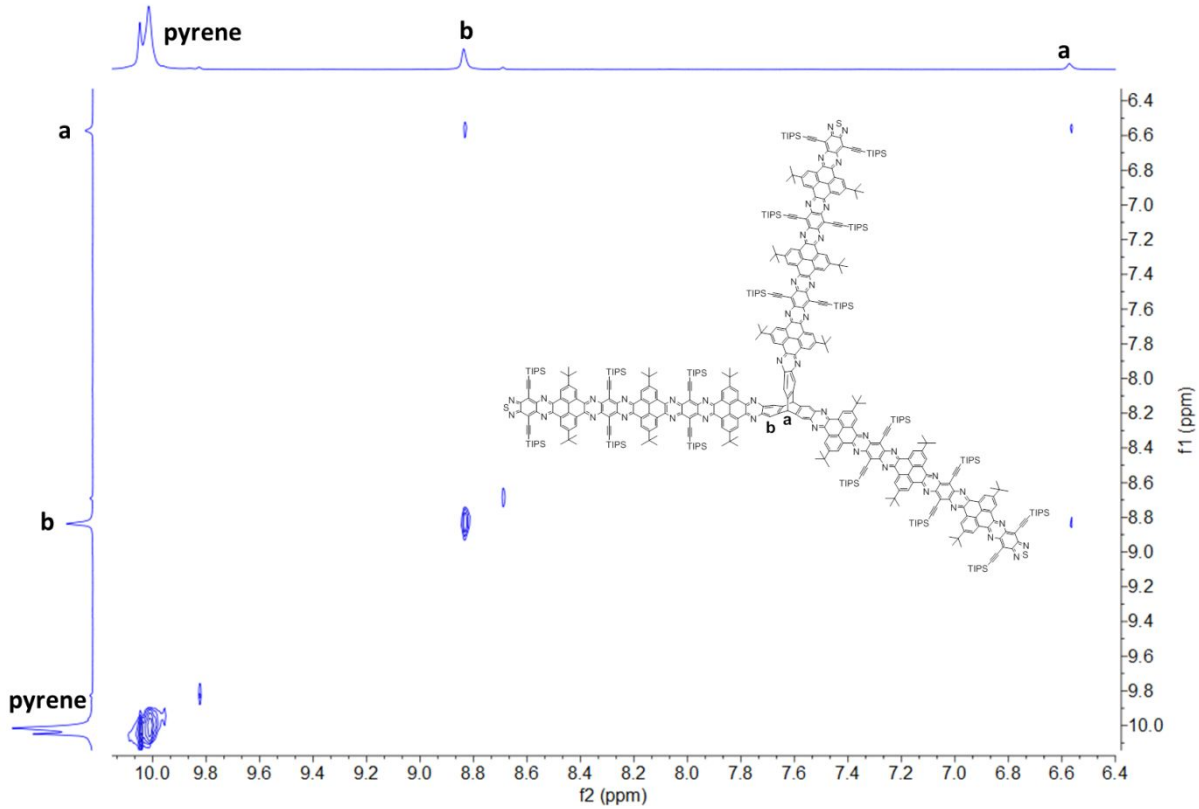

Figure S15. Aromatic region of the ^{1}H–^{1}H NOESY spectrum of compound **P3** in TCE-d_2 on 500 MHz at 413 K.

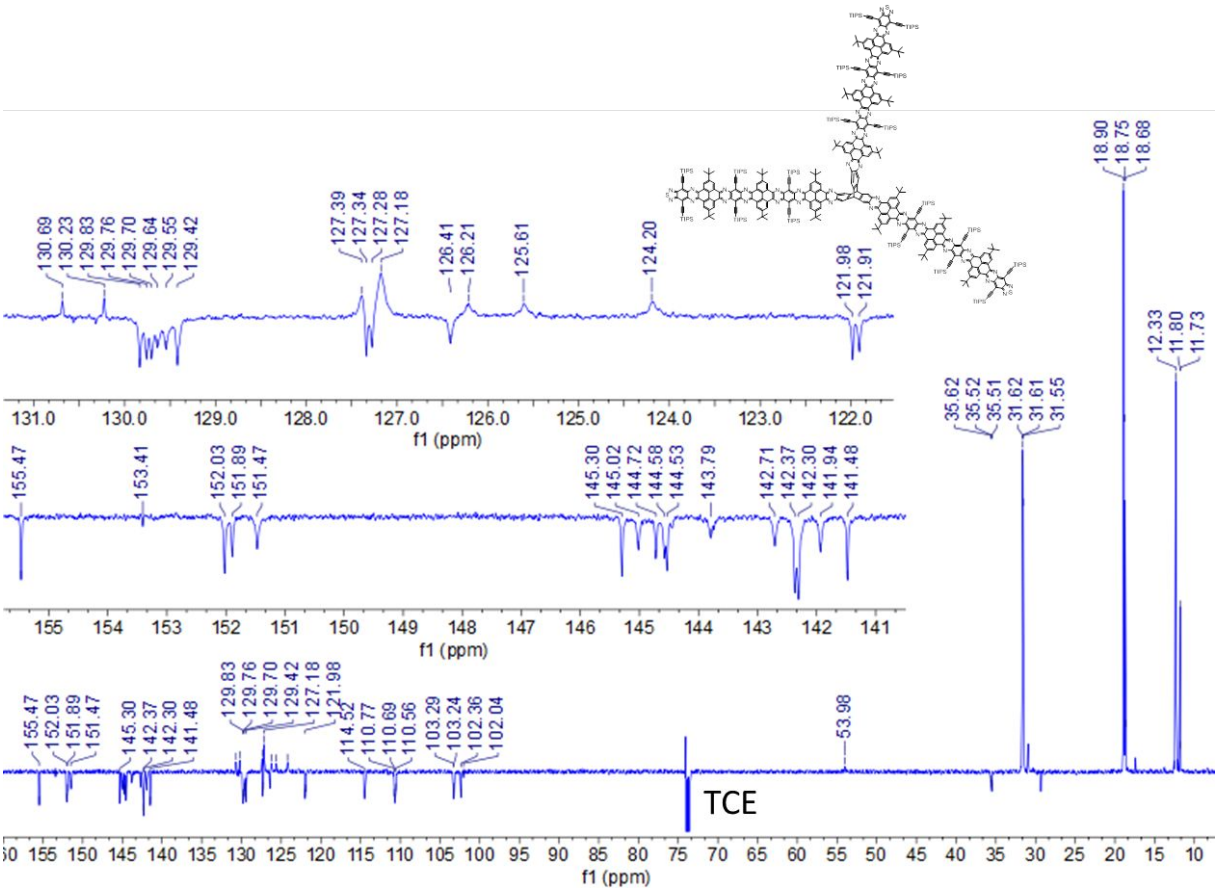

Figure S16. The APT ^{13}C NMR spectrum of compound **P3** in TCE-d_2 on 125 MHz at 413 K.

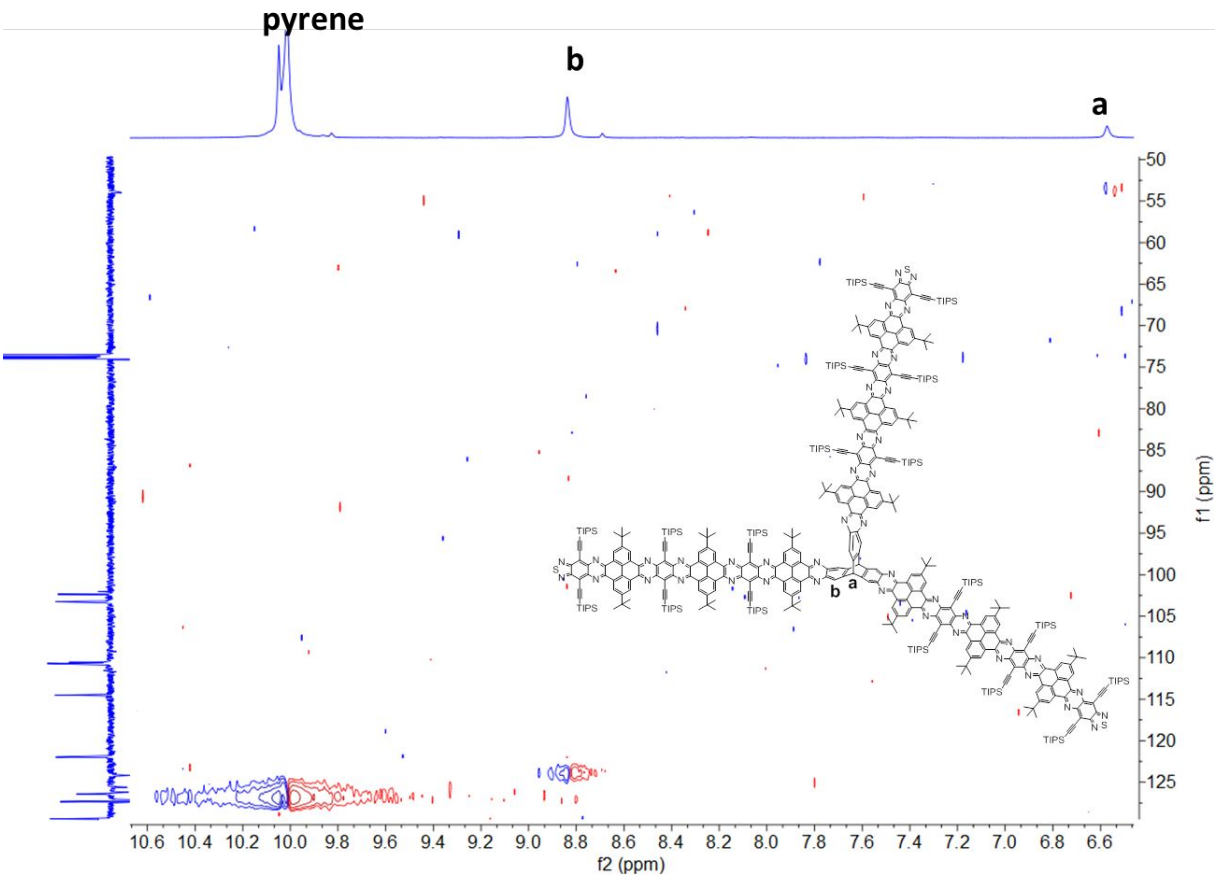

Figure S17. The aromatic region of the ^{1}H-^{13}C HSQC spectrum of compound **P3** TCE-d_2 at 413 K.

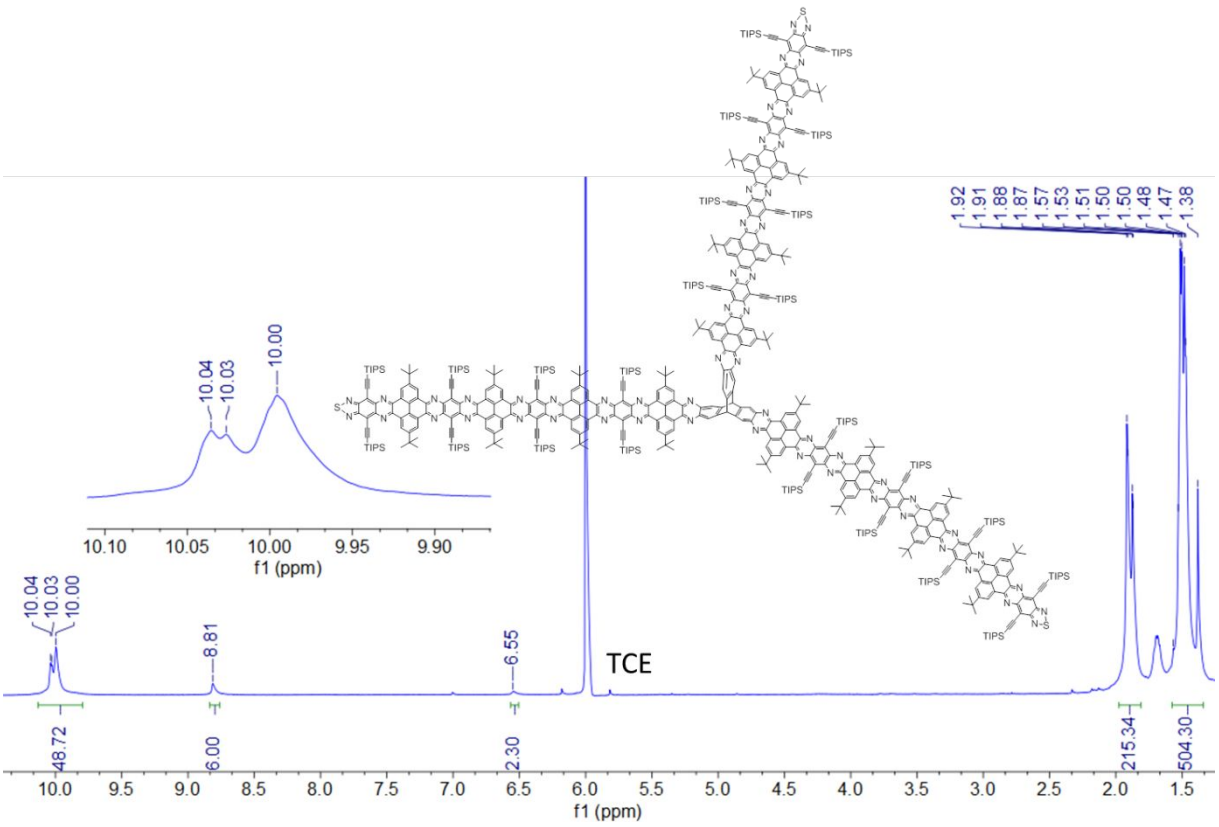

Figure S18. The ^{1}H NMR spectrum of compound **P4** in TCE-d_2 on 500 MHz at 413 K.

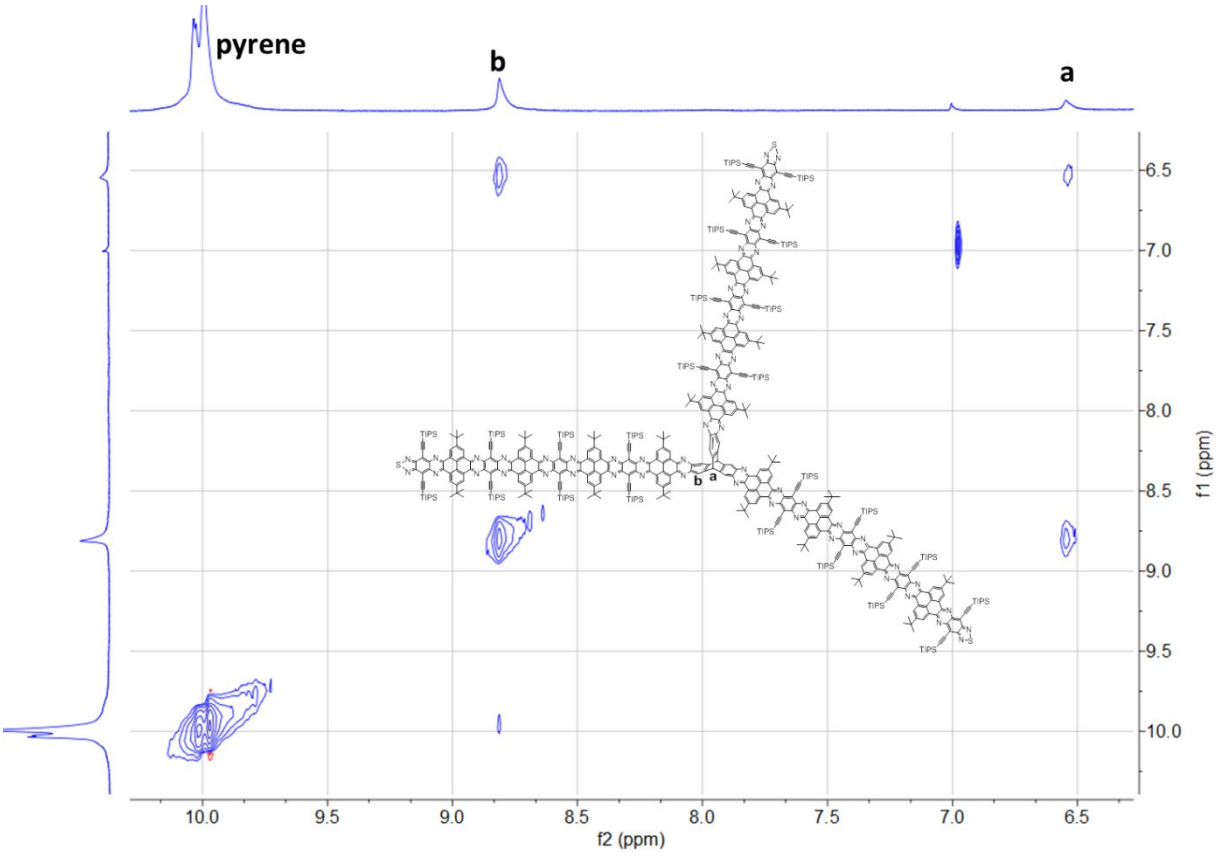

Figure S19. Aromatic region of the ^{1}H–^{1}H NOESY spectrum of compound **P4** in TCE-d_2 on 500 MHz at 413 K.

Maldi-TOF MS

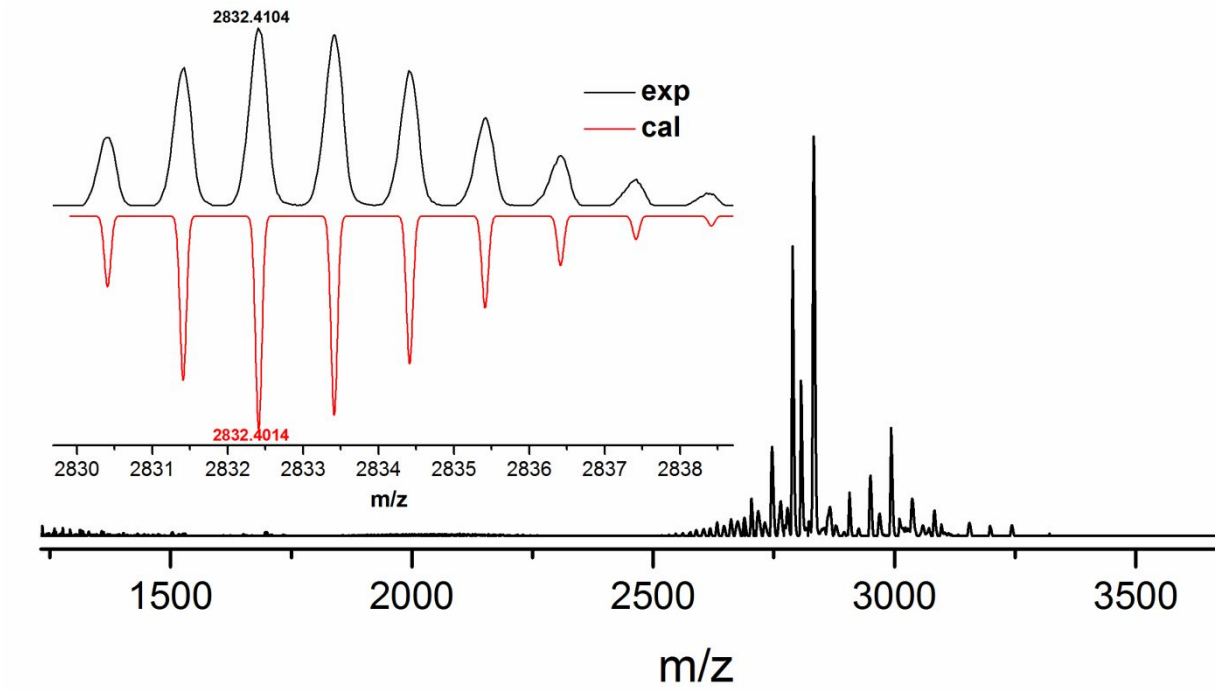

Figure S20. The MALDI-TOF MS of **P1** ($[M+H]^+$).

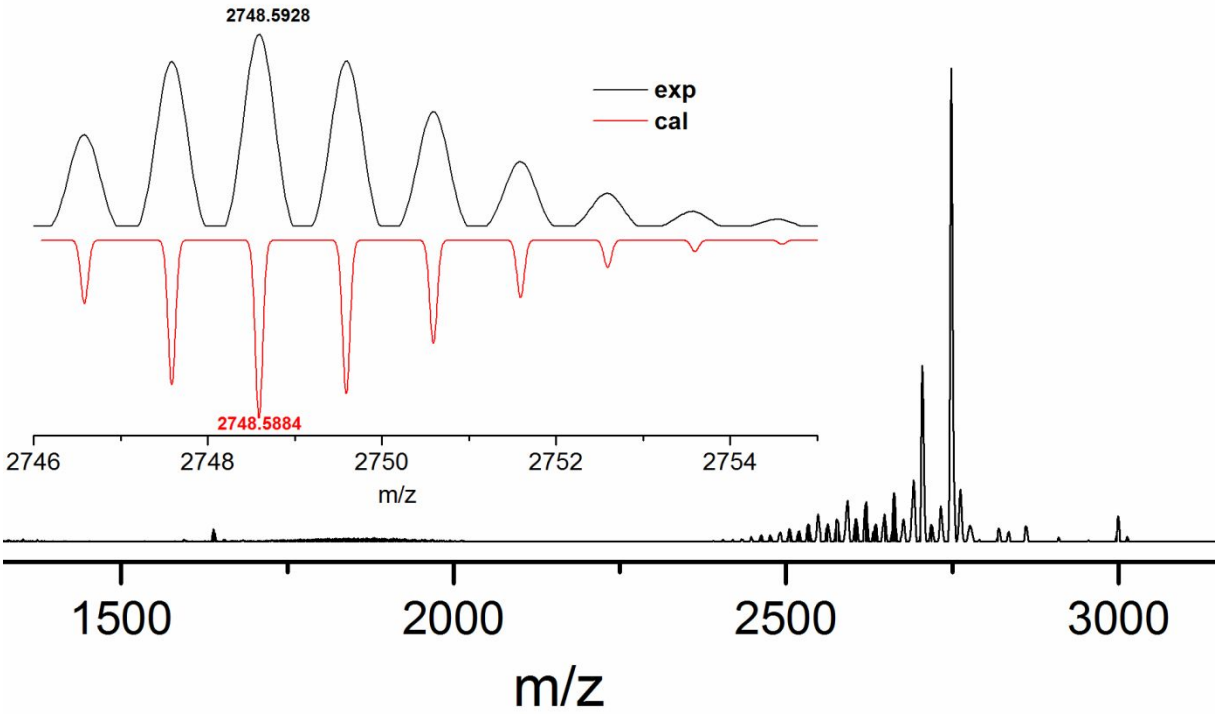

Figure S21. The MALDI-TOF MS of **M1** ($[M+H]^+$).

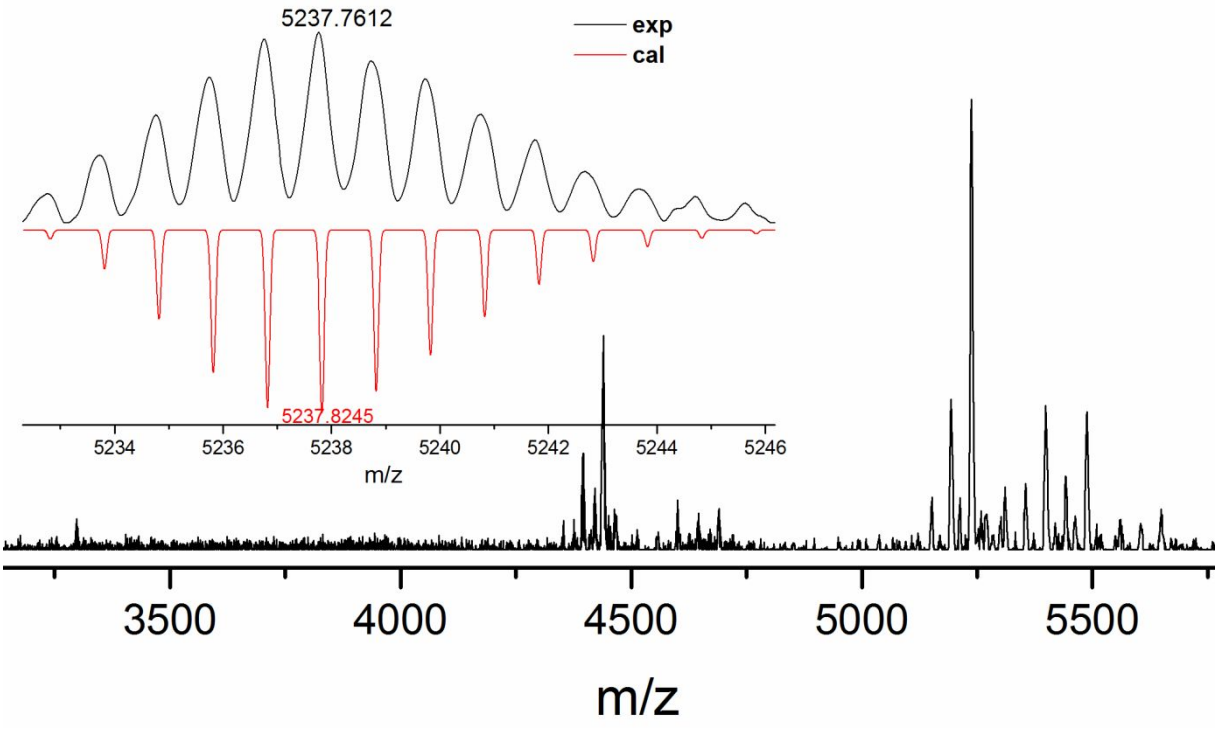

Figure S22. The MALDI-TOF MS of **P2** ($[M+2H]^+$).

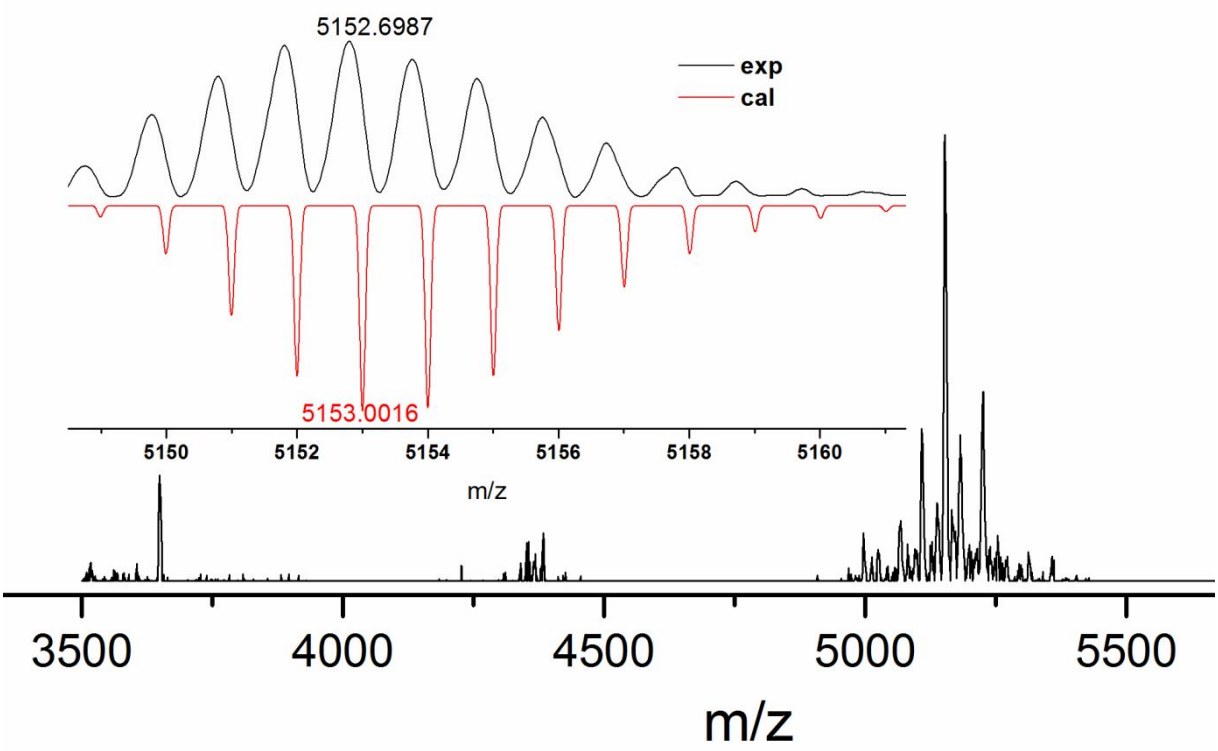

Figure S23. The MALDI-TOF MS of **M2** ($[M+H]^+$).

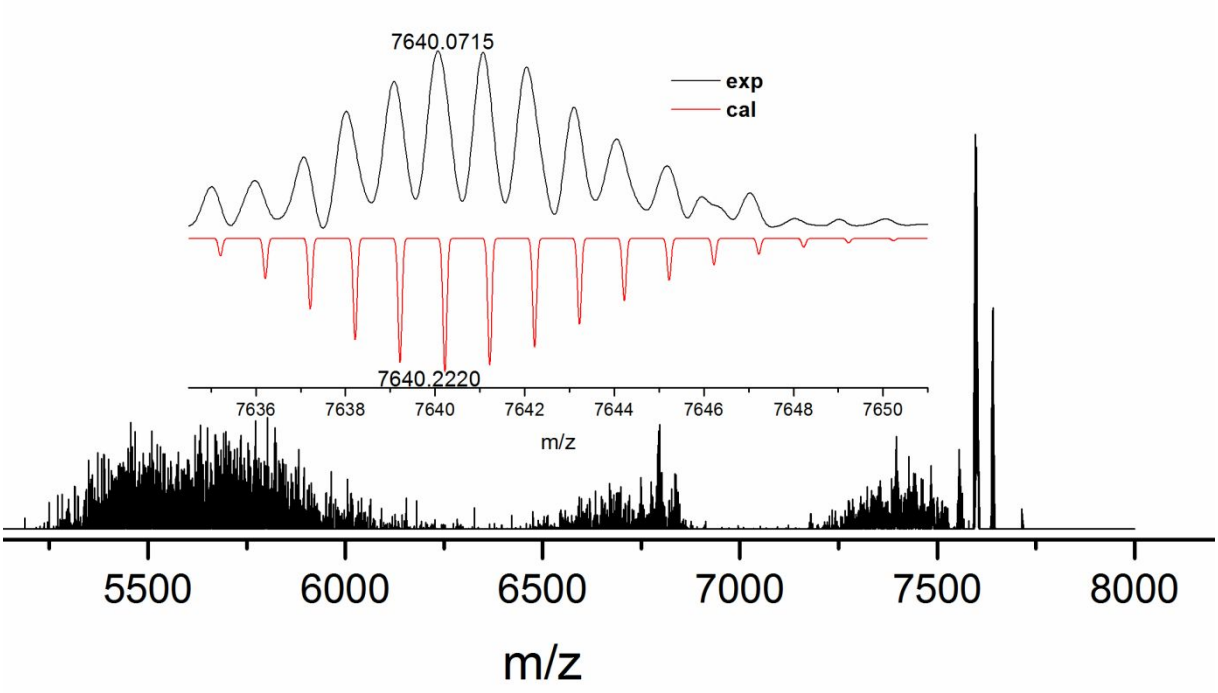

Figure S24. The MALDI-TOF MS of **P3** ($[M+H]^+$).

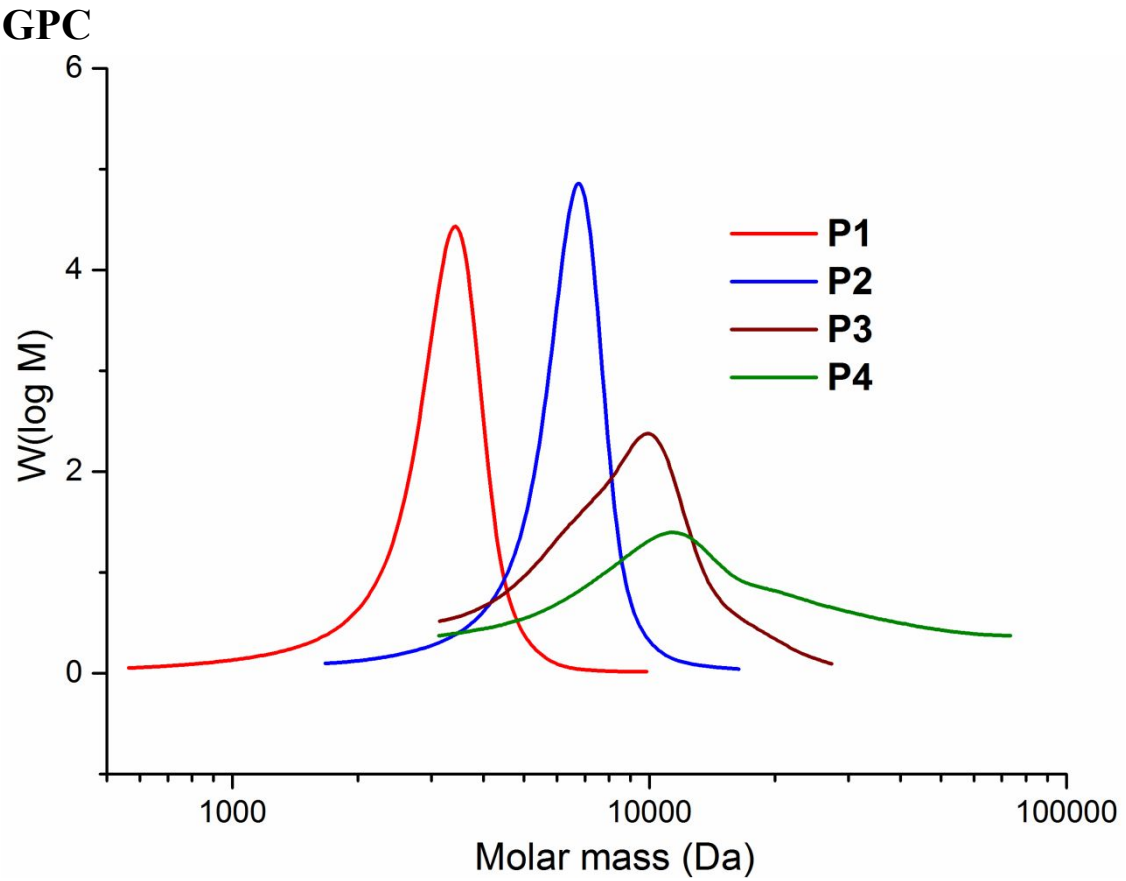

Figure S25. The GPC curves of P1-P4.

	Mn[a]	Mw[b]	PDI[c]
P1	2762.53	3151.59	1.14
P2	5743.73	6337.77	1.10
P3	7628.39	9246.88	1.21
P4	10647.5	18459.70	1.73

[a] *M*n = number average molecular weight; [b] *M*w = weight average molecular weight; [c]PDI = poly dispersity index.

DFT calculation

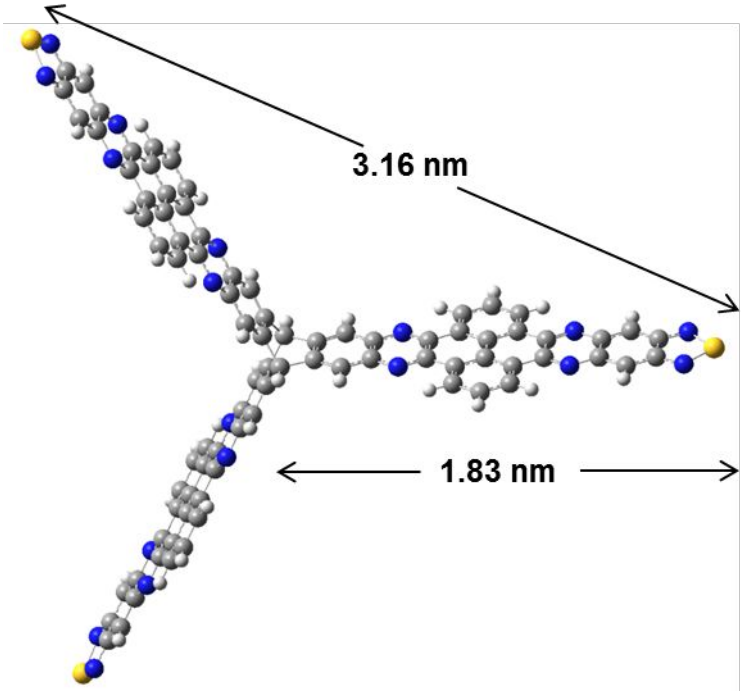

Figure S26. Structure and geometry of **P1** at the B3LYP/6-31G level.

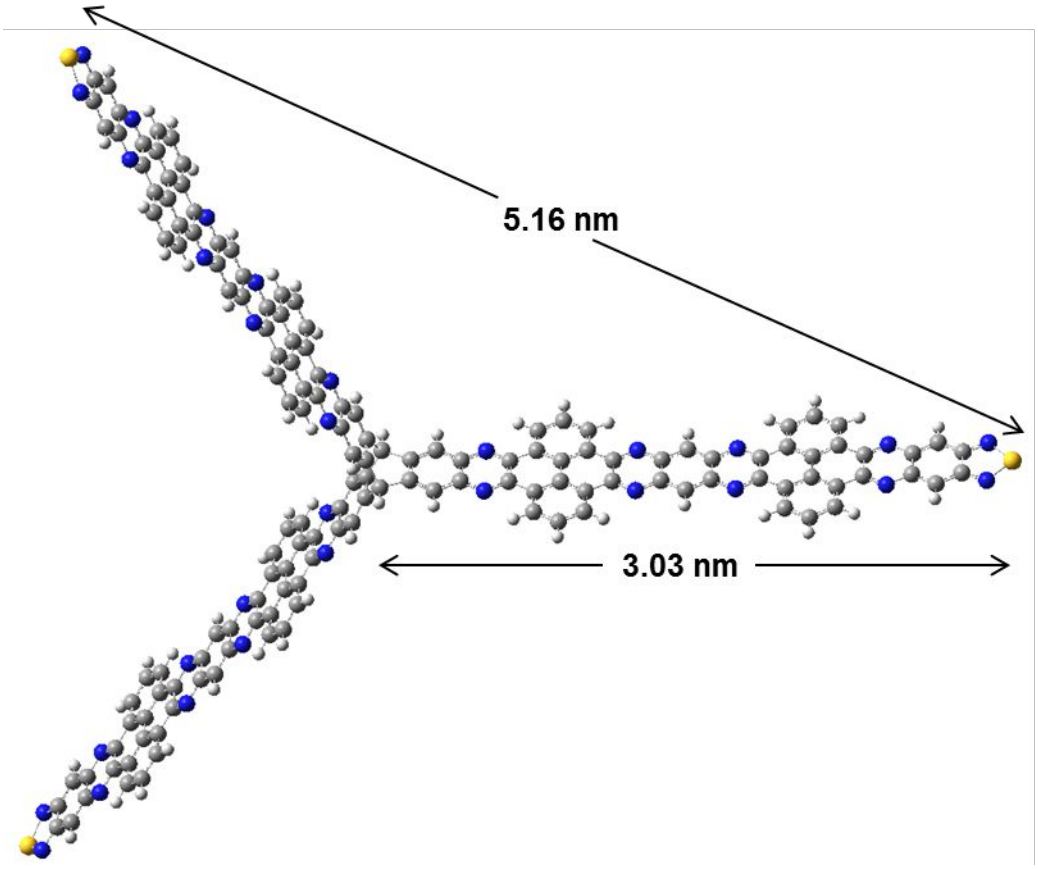

Figure S27. Structure and geometry of **P2** at the B3LYP/6-31G level.

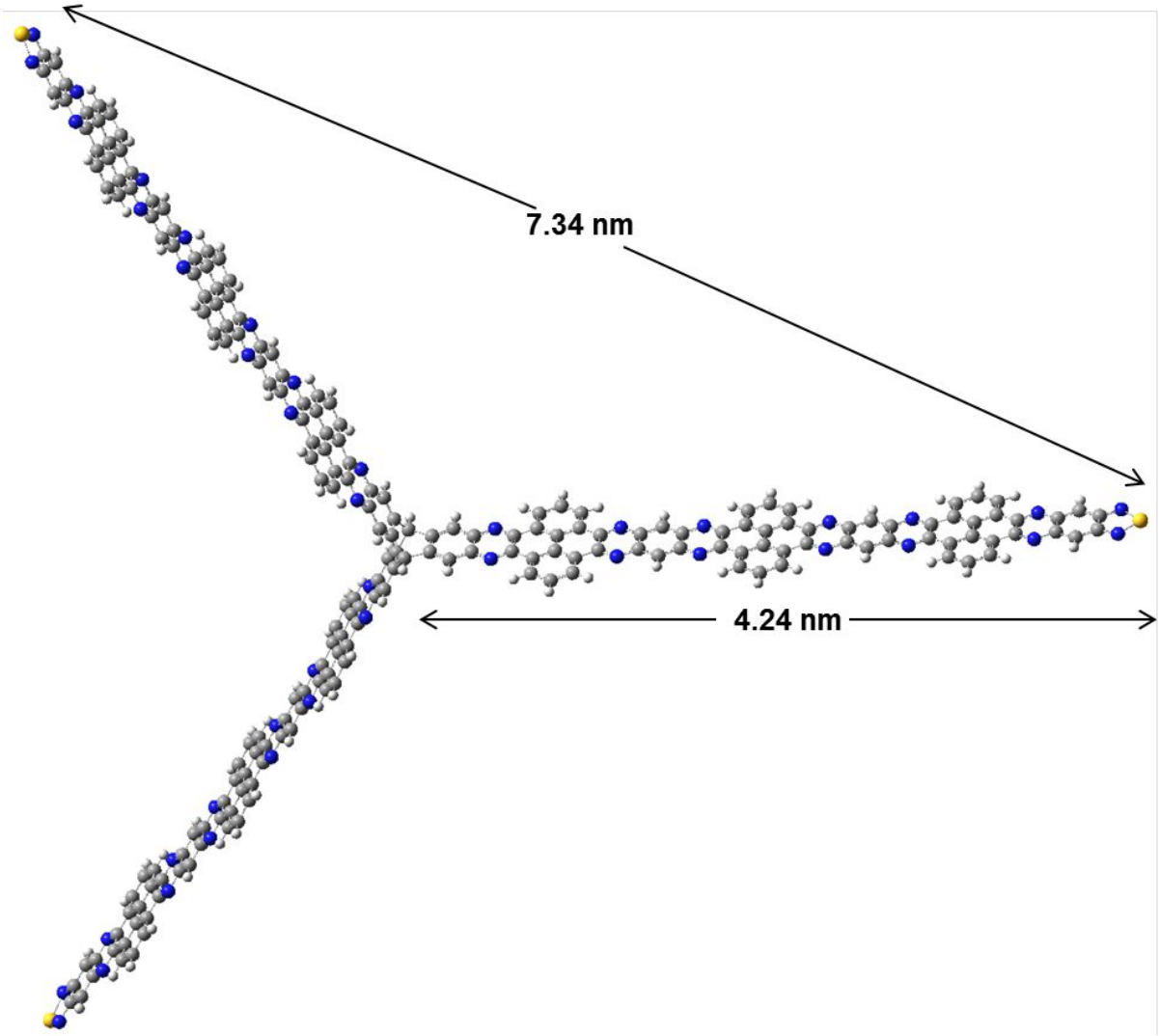

Figure S28. Structure and geometry of **P3** at the B3LYP/6-31G level.

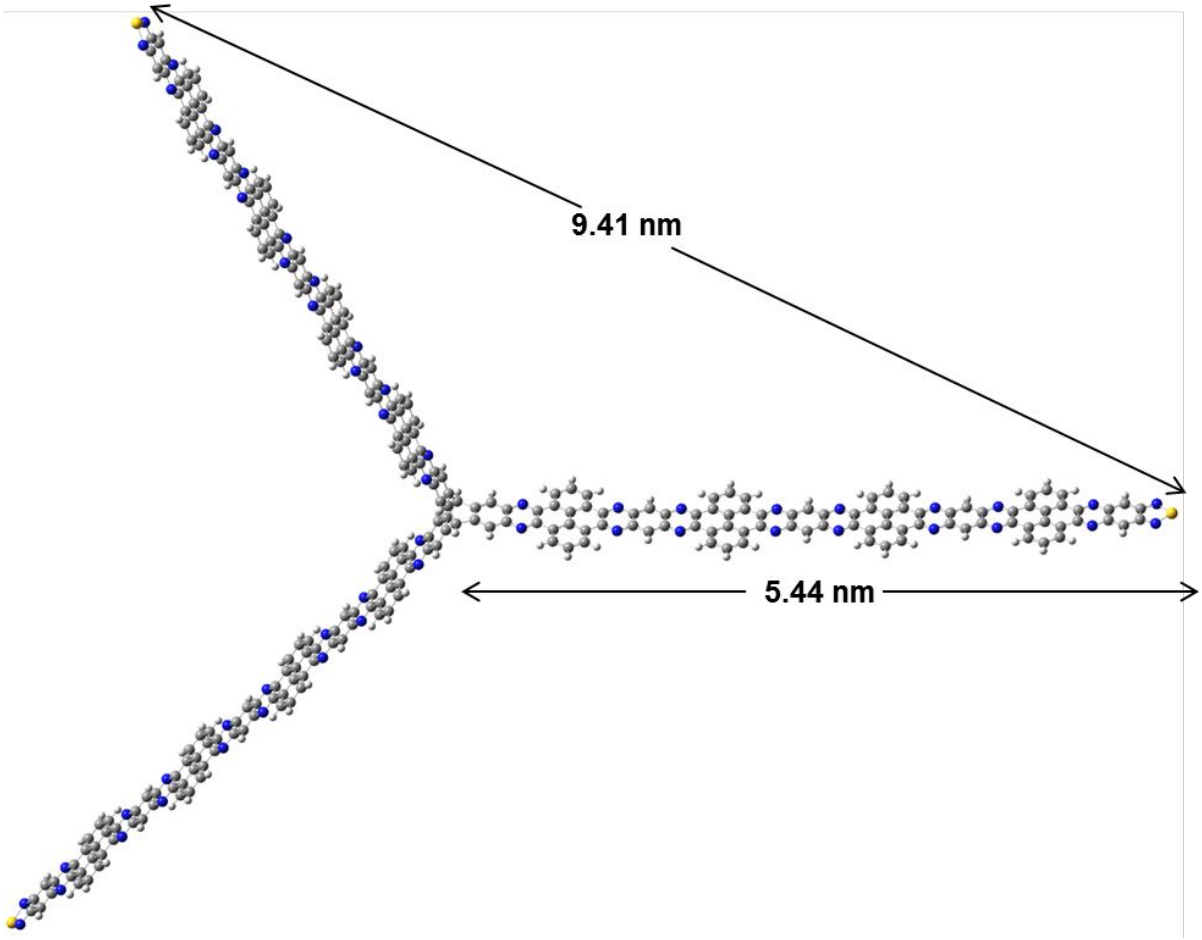

Figure S29. Structure and geometry of **P4** at the B3LYP/6-31G level.

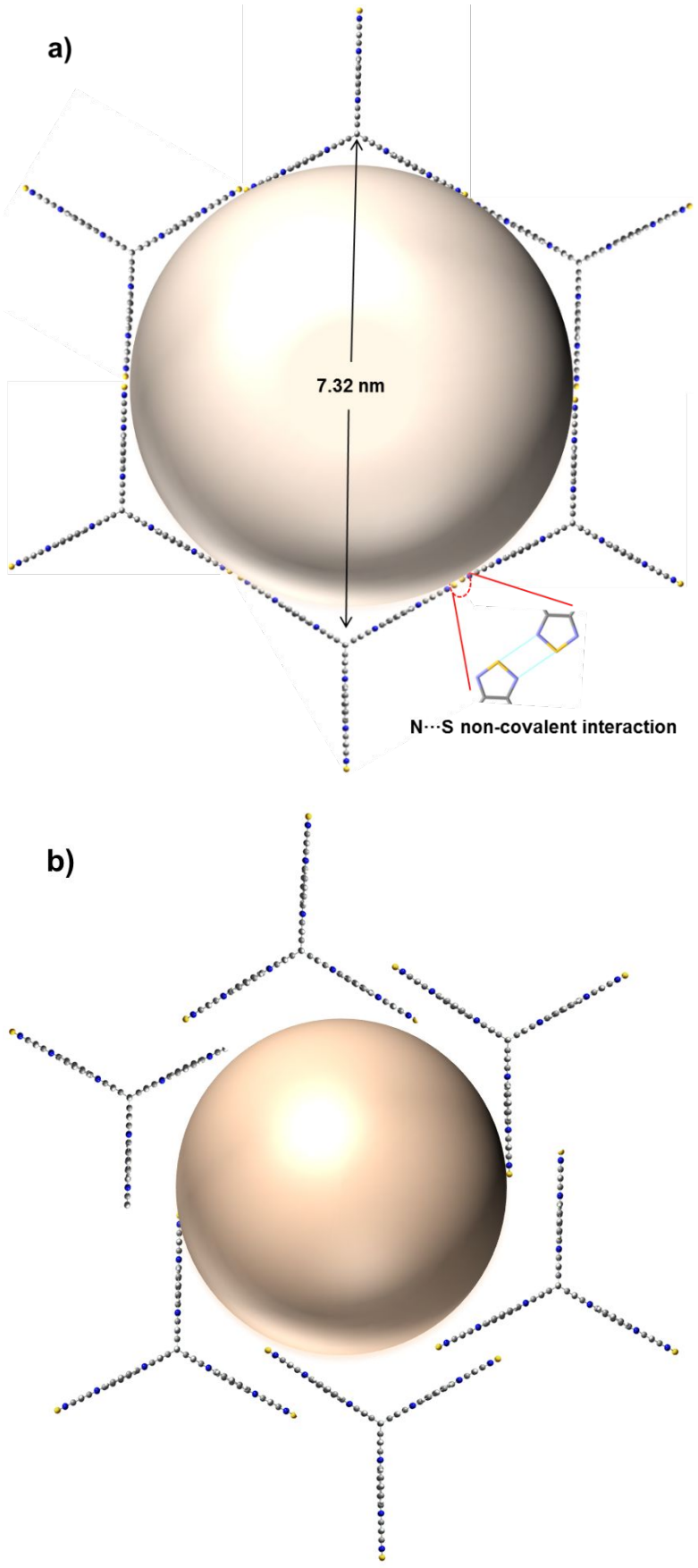

Figure S30. The possible packing structures by N-S noncovalent interaction (a) and π-π interaction (b) in the crystal.

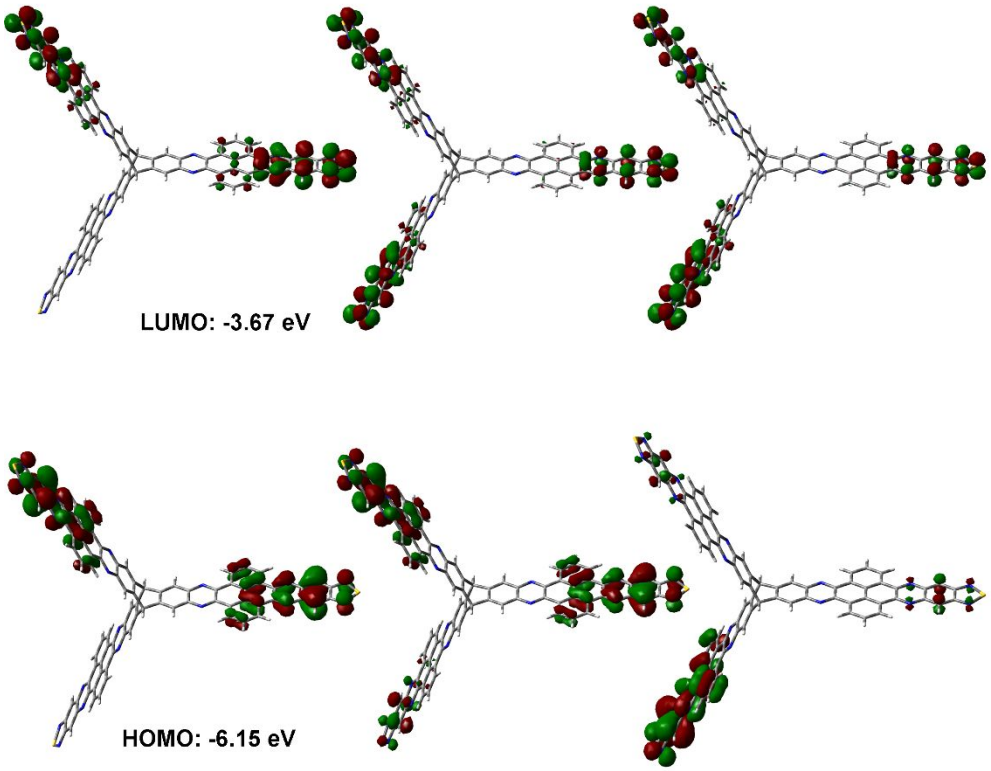

Figure S31. Frontier orbitals of **P1** computed with B3LYP/6-31G.

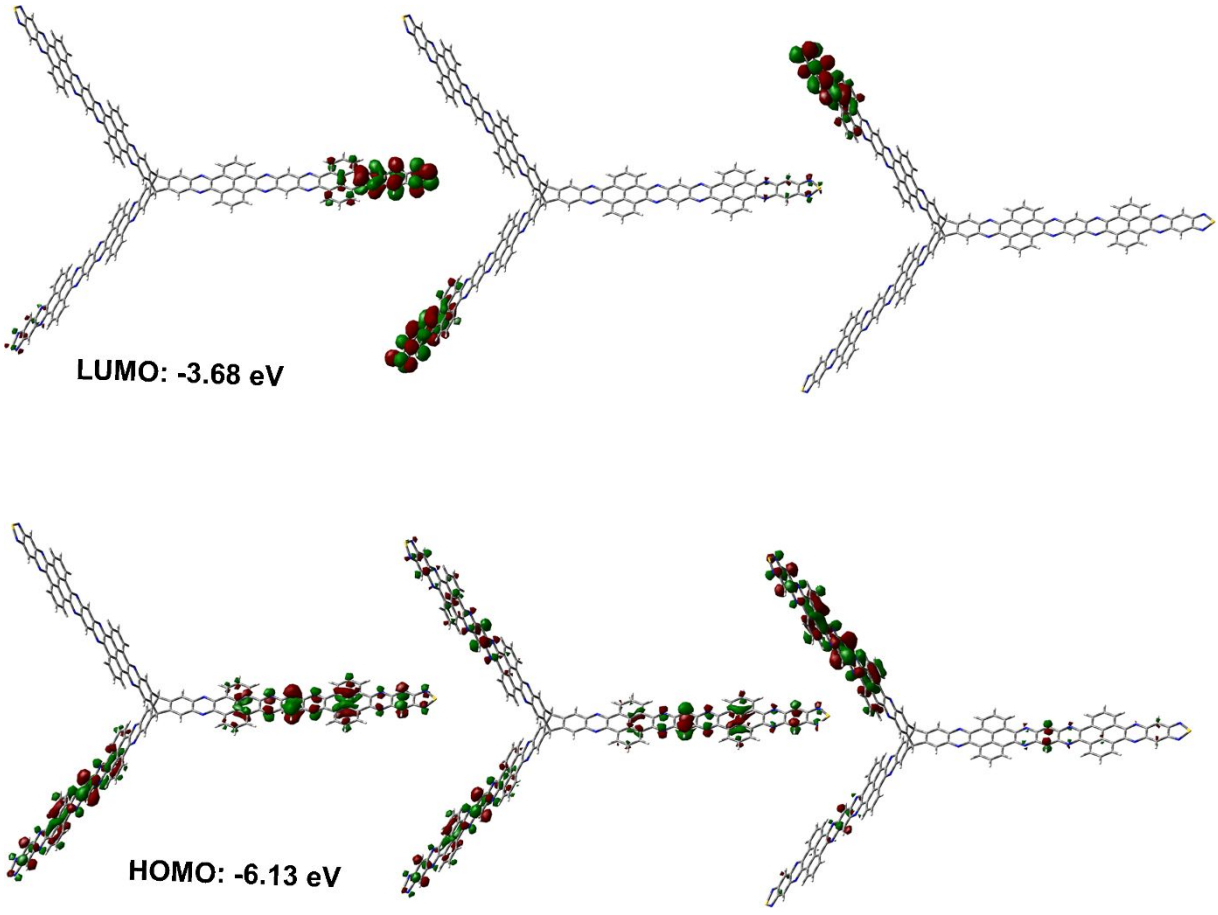

Figure S32. Frontier orbitals of **P2** computed with B3LYP/6-31G.

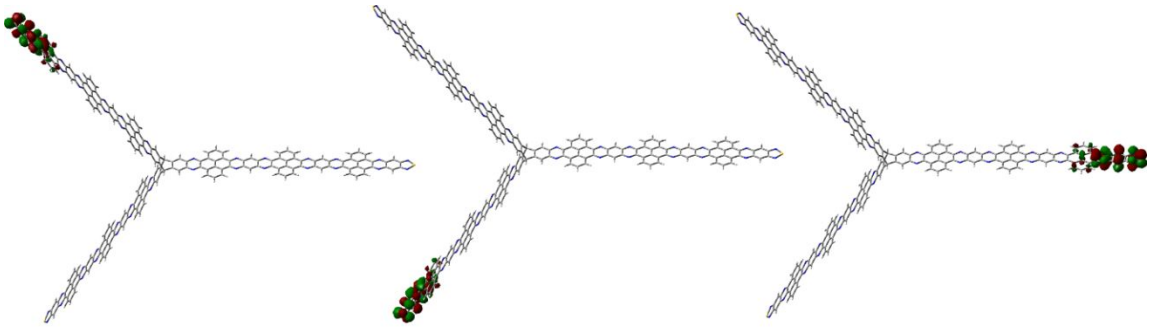

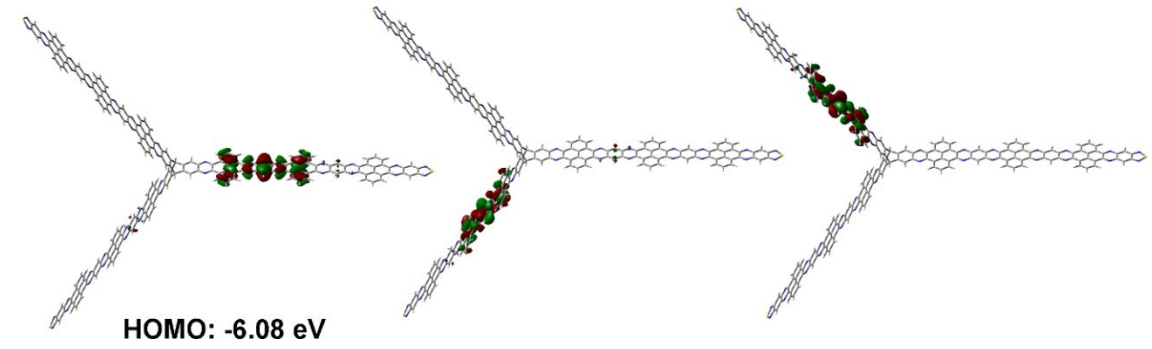

Figure S33. Frontier orbitals of **P3** computed with B3LYP/6-31G.

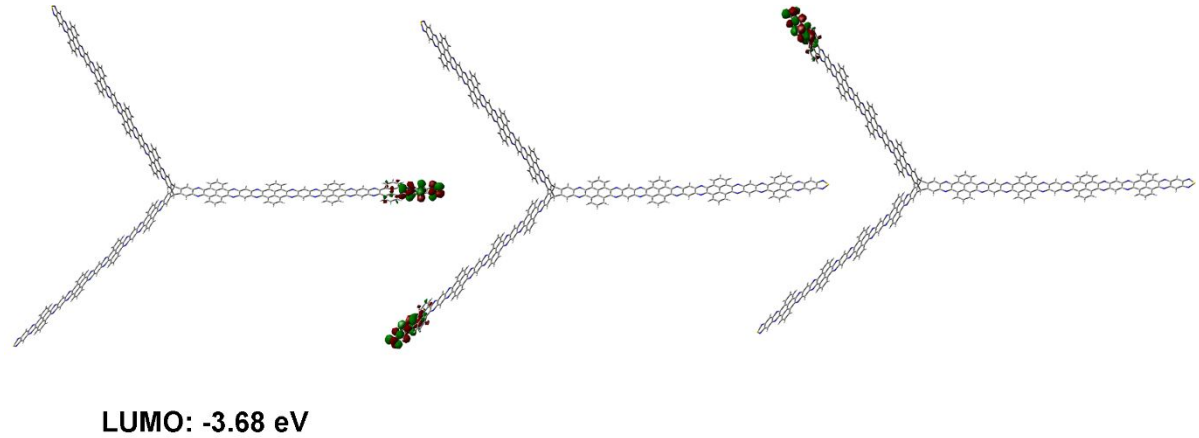

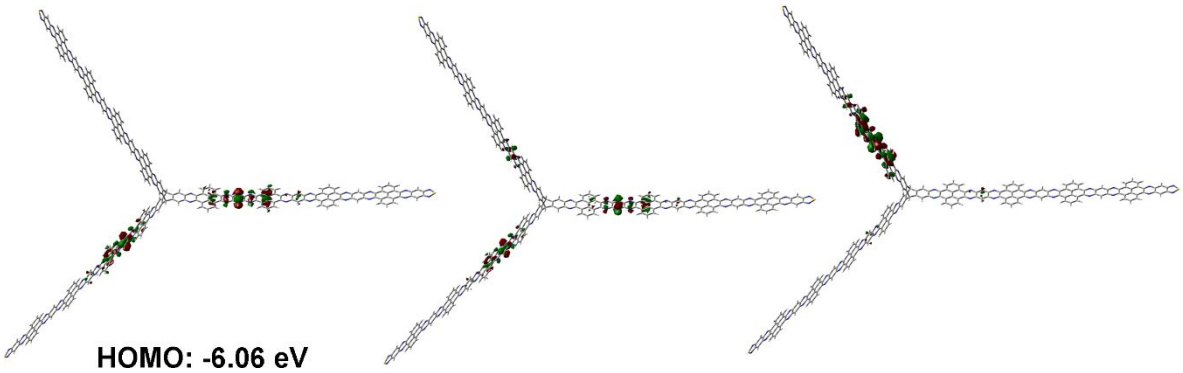

Figure S34. Frontier orbitals of **P4** computed with B3LYP/6-31G.

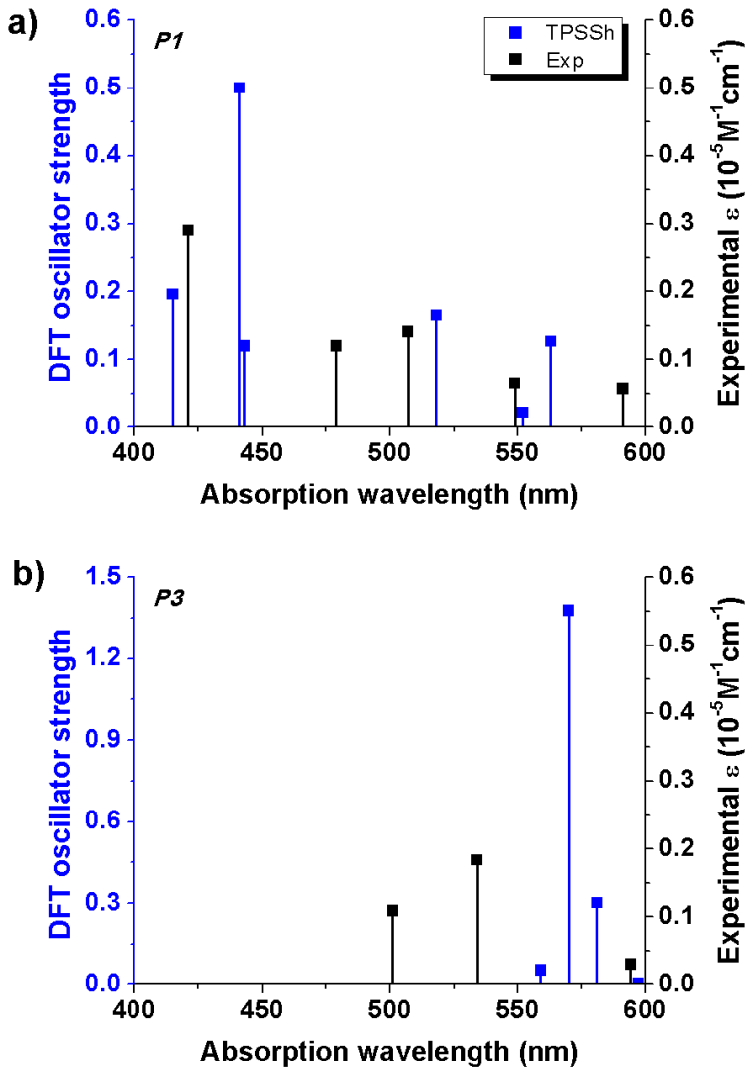

Figure S35. The TD-TPSSh/6-31G(d)/PCM(THF) calculated electronic absorption transitions corresponding to (a) the five longest-wavelength maxima of **P1** and (b) the two longest-wavelength maxima of **P3**; the computed transitions are compared to the experimental data taken from Figure 2a of the main manuscript

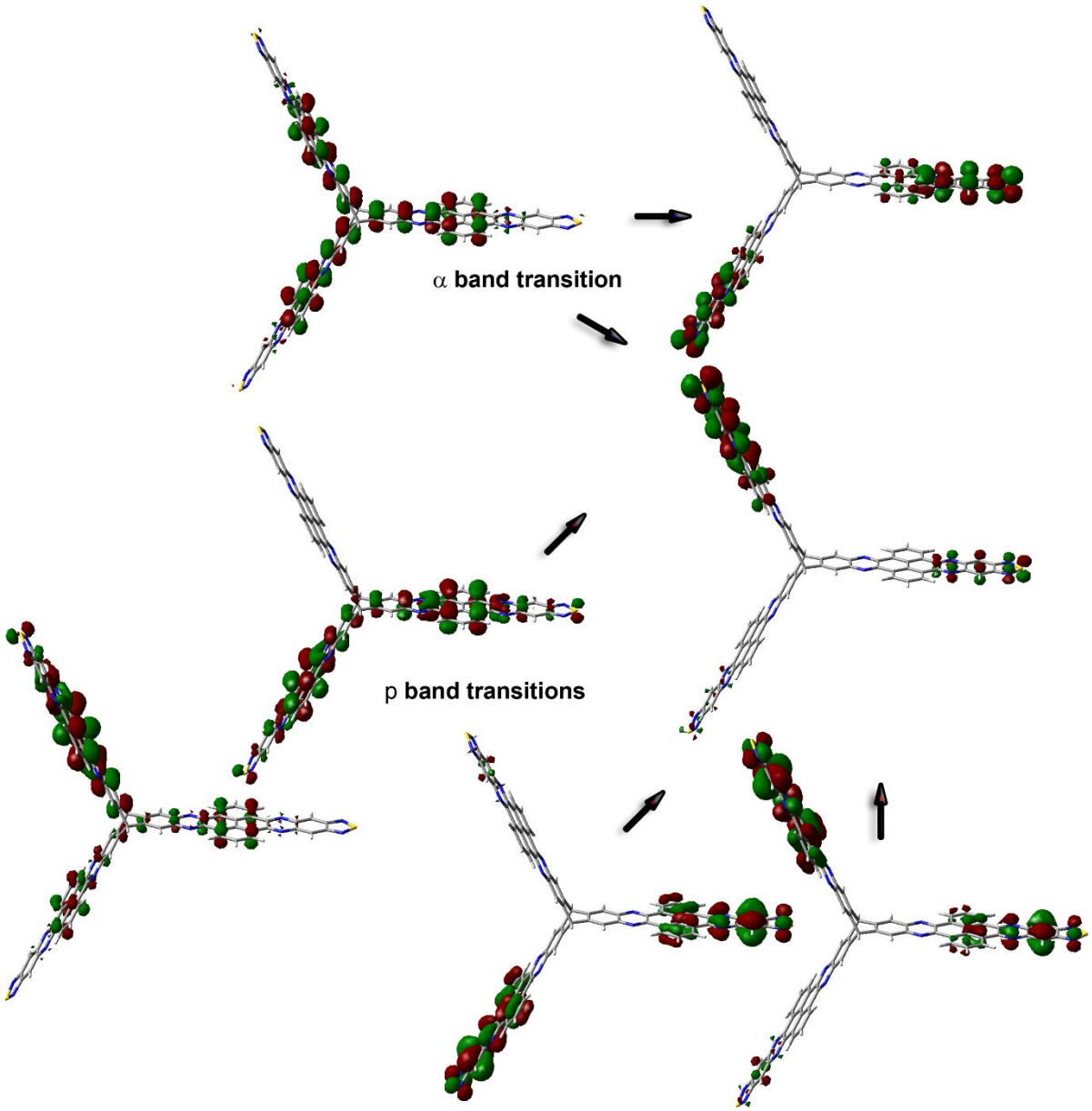

Figure S36. MOs involved in the three longest-wavelength electronic absorption transitions calculated with TD-TPSSh/6-31G(d)/PCM(THF) for **P1.**

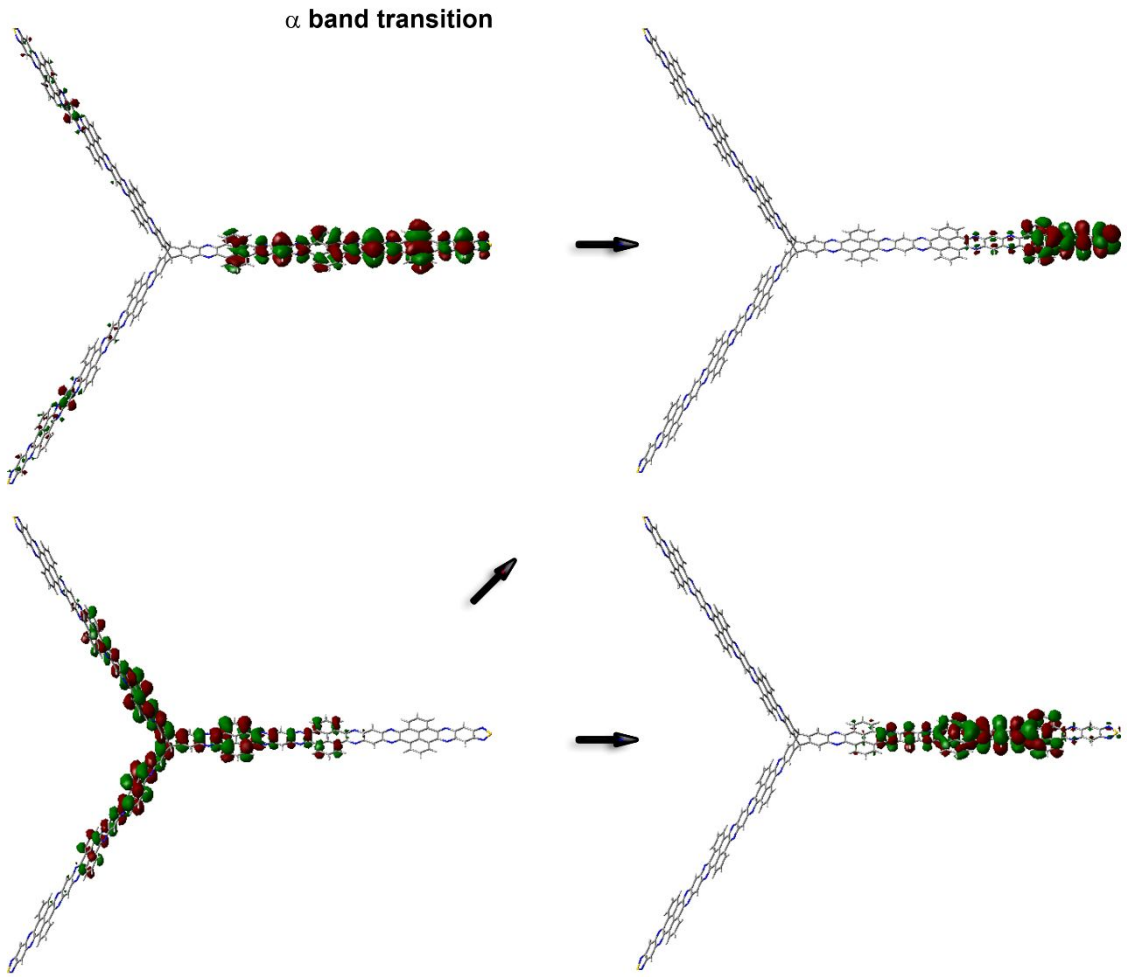

Figure S37. MOs involved in the three longest-wavelength electronic absorption transitions calculated with TD-TPSSh/6-31G(d)/PCM(THF) for **P3.**

References

S1. Becke, A. D. Density-functional exchange-energy approximation with correct asymptotic behavior. *Phys. Rev. A: At., Mol., Opt. Phys.*, **1988**, *38*, 3098–3100.

S2. Lee, C.; Yang, W.; Parr, R. G. Development of the Colle-Salvetti correlation-energy formula into a functional of the electron density. *Phys. Rev. B: Condens. Matter Mater. Phys.*, **1988**, *37*, 785–789.

S3. Gaussian 09, Revision D.01, Frisch, M. J.; Trucks, G. W.; Schlegel, H. B.; Scuseria, G. E.; Robb, M. A.; Cheeseman, J. R.; Scalmani, G.; Barone, V.; Mennucci, B.; Petersson, G. A.; Nakatsuji, H.; Caricato, M.; Li, X.; Hratchian, H. P.; Izmaylov, A. F.; Bloino, J.; Zheng, G.; Sonnenberg, J. L.; Hada, M.; Ehara, M.; Toyota, K.; Fukuda, R.; Hasegawa, J.; Ishida, M.; Nakajima, T.; Honda, Y.; Kitao, O.; Nakai, H.; Vreven, T.; Montgomery, J. A.; Peralta, J. E.; Ogliaro, F.; Bearpark, M.; Heyd, J. J.; Brothers, E.; Kudin, K. N.; Staroverov, V. N.; Kobayashi, R.; Normand, J.; Raghavachari, K.; Rendell, A.; Burant, J. C.; Iyengar, S. S.; Tomasi, J.; Cossi, M.; Rega, N.; Millam, J. M.; Klene, M.; Knox, J. E.; Cross, J. B.; Bakken, V.; Adamo, C.; Jaramillo, J.; Gomperts, R.; Stratmann, R. E.; Yazyev, O.; Austin, A. J.; Cammi, R.; Pomelli, C.; Ochterski, J. W.; Martin, R. L.; Morokuma, K.; Zakrzewski, V. G.; Voth, G. A.; Salvador, P.; Dannenberg, J. J.; Dapprich, S.; Daniels, A. D.; Farkas, O.; Foresman, . V.; Cioslowski, J.; and Fox, D. J. Gaussian, Inc., Wallingford CT, 2013.J. B.; Ortiz, J

S4. Gaussian 16, Revision B.01, Frisch, M. J.; Trucks, G. W.; Schlegel, H. B.; Scuseria, G. E.; Robb, M. A.; Cheeseman, J. R.; Scalmani, G.; Barone, V.; Petersson, G. A.; Nakatsuji, H.; Li, X.; Caricato, M.; Marenich, A. V.; Bloino, J.; Janesko, B. G.; Gomperts, R.; Mennucci, B.; Hratchian, H. P.; Ortiz, J. V.; Izmaylov, A. F.; Sonnenberg, J. L.; Williams-Young, D.; Ding, F.; Lipparini, F.; Egidi, F.; Goings, J.; Peng, B.; Petrone, A.; Henderson, T.; Ranasinghe, D.; Zakrzewski, V. G.; Gao, J.; Rega, N.; Zheng, G.; Liang, W.; Hada, M.; Ehara, M.; Toyota, K.; Fukuda, R.; Hasegawa, J.; Ishida, M.; Nakajima, T.; Honda, Y.; Kitao, O.; Nakai, H.; Vreven, T.; Throssell, K.; Montgomery, J. A.; Peralta, Jr., J. E.; Ogliaro, F.; Bearpark, M. J.; Heyd, J. J.; Brothers, E. N.; Kudin, K. N.; Staroverov, V. N.; Keith, T. A.; Kobayashi, R.; Normand, J.; Raghavachari, K.; Rendell, A. P.; Burant, J. C.; Iyengar, S. S.; Tomasi, J.; Cossi, M.; Millam, J. M.; Klene, M.; Adamo, C.; Cammi, R.; Ochterski, J. W.; Martin, R. L.; Morokuma, K.; Farkas, O.; Foresman, J. B.; Fox, D. J. Gaussian, Inc., Wallingford CT, 2016.

S5. Tao, J. M.; Perdew, J. P.; Staroverov, V. N.; Scuseria, G. E. Climbing the Density Functional Ladder: Nonempirical Meta–Generalized Gradient Approximation Designed for Molecules and Solids. *Phys. Rev. Lett.* **2003**, *91*, 146401.

S6. Tomasi, J.; Mennucci, B.; Cammi, R. Quantum mechanical continuum solvation models. *Chem. Rev.* **2005**, *105*, 2999-3094.

S7. Hu B.-L.; Zhang, K.; An, C.; Schollmeyer, D.; Pisula, W.; Baumgarten, M. Layered Thiadiazoloquinoxaline-Containing Long Pyrene-Fused N-Heteroacenes. *Angew. Chem. In. Ed.* **2018**, *57*, 12375-12379.

S8. An, C.; Zhou, S.; Baumgarten, M. Condensed Derivatives of Thiadiazoloquinoxaline as Strong Acceptors. *Cryst. Growth Des.* **2015**, *15*, 1934-1938.

S9. Cortizo-Lacalle, D.; Pertegas, A.; Melle-Franco, M.; Bolink, H. J.; Mateo-Alonso, A. Pyrene-fused bisphenazinothiadiazoles with red to NIR electroluminescence. *Org. Chem. Front.* **2017**, *4*, 876-881.